

Development of Kinetic Energy Density Functional Using Response Function Defined on the Energy Coordinate

Hideaki Takahashi*

March 2, 2022

Abstract

A kinetic energy functional E_{kin}^e was developed within the framework of the density-functional theory (DFT) based on the energy electron density for the purpose of realizing the orbital-free DFT. The functional includes the nonlocal term described with the linear-response function (LRF) of a reference system. As a notable feature of the present approach, the LRF is represented on the energy coordinate ϵ defined for each system of interest. In addition, an atomic system is taken as a reference system for the construction of the LRF, which shows a clear difference from the conventional approach based on the homogeneous electron gas. The explicit form of the functional E_{kin}^e was formulated by means of the coupling-parameter integration scheme. The functional E_{kin}^e was applied to the calculations of the kinetic energies of the pseudo atoms that mimics H, He, Ne, and Ar. Explicitly, the kinetic energy of each atom was computed using the functional E_{kin}^e with respect to the variation of the valence charge Z_v of each atom. In these calculations, the electron density n optimized by the Kohn-Sham DFT was adopted as an argument of the functional. It was found that the results are in excellent agreements with those given by the Kohn-Sham DFT. We also devised a method to perform the self-consistent field calculation utilizing the functional E_{kin}^e . The method was applied to the computation of the radial distribution functions of the electrons in the pseudo Ne and Ar atoms. It was demonstrated that the results reasonably agree with those yielded by the Kohn-Sham DFT.

*Department of Chemistry, Graduate School of Science, Tohoku University, Sendai, Miyagi 980-8578, Japan

1 Introduction

Density-functional theory (DFT) for electrons[1] is one of the principal subjects in modern physics and chemistry. It offers an efficient and robust theoretical framework to study electronic structures of materials and molecules[2]. Vast amounts of effort have been devoted to the developments of functionals and to the foundation of the theoretical basis of DFT[3]. Nowadays, DFT is an indispensable tool in the computational approach to the material design and molecular synthesis because of its efficiency and reliability. In the early study of DFT it was proved in formulation[1, 4] that there exists an exact universal functional $E[n]$ that describes the total energy E in terms of the N -representable[1, 4] electron density n . However, the Kohn-Sham (KS) method[1, 5], which has so far been the only workhorse in the DFT, utilizes one-electron orbitals as the variables in the variational search. The introduction of the wave functions in KS-DFT is necessitated to ensure the accurate evaluation of the kinetic energy of the electrons. However, it gives rise to the computational cost associated with the orthogonalization among the orbitals, which roughly scales as $O(N^3)$ with the system size N . If the construction of an effective kinetic energy functional is made possible, the one-electron orbitals become no longer necessary, and consequently, the computational cost scales linearly with the system size (‘Order- N ’) since the orthogonalization can be completely bypassed in the variational calculations. Thus, it is a matter of great significance in physics and chemistry to develop the efficacious orbital-free DFT (OF-DFT) to extend the frontier of the applications of DFT[6].

Development of an accurate kinetic energy density functional $E_{\text{kin}}[n]$ is, however, known as the toughest subject. A primitive approximation to $E_{\text{kin}}[n]$ was first given in 1928 by Thomas and Fermi (TF)[7, 8] using the homogeneous electron gas (HEG)[1] as a reference system. For the total electron density n , the TF functional $E_{\text{TF}}[n]$ has the form

$$E_{\text{TF}}[n] = C_{\text{TF}} \int d\mathbf{r} n(\mathbf{r})^{\frac{5}{3}} \quad (1)$$

where $C_{\text{TF}} = \frac{3}{10} (3\pi^2)^{\frac{2}{3}}$ and \mathbf{r} is the position vector of the electrons. In 1935 a gradient correction $E_{\text{vW}}[n]$

$$E_{\text{vW}}[n] = -\frac{1}{2} \int d\mathbf{r} n(\mathbf{r})^{1/2} \nabla^2 n(\mathbf{r})^{1/2} \quad (2)$$

was made by von Weizsäcker.[9] It is readily recognized that Eq. (2) by itself is an exact $E_{\text{kin}}[n]$ for one or two electrons systems. Inclusion of $E_{\text{vW}}[n]$ with a prefactor λ (λvW)

$$E_{\text{TFW}}[n] = E_{\text{TF}}[n] + \lambda E_{\text{vW}}[n] \quad (3)$$

makes a substantial contribution to reduce errors. The behavior of the linear response function(LRF) of $E_{\text{TFW}}[n]$ in the momentum space was analyzed, for instance, in Ref. [10]. It shows that LRF of $E_{\text{TFW}}[n]$ with $\lambda = 1$ reproduces the asymptotic behavior of the HEG in the large \mathbf{k} limit, while setting $\lambda = 1/9$ realizes that in the small \mathbf{k} region. As demonstrated in Ref. [11], $\lambda = 1/5$ gives the best results when it is applied to atoms. Unfortunately, higher order corrections to $E_{\text{TFW}}[n]$ offers quite minor improvements at the most. It has long been considered that the deficiency of these local and semilocal kinetic operators is that they would not be able to realize the shell structures of electron densities in atoms. This motivated the introduction of the nonlocal term in the functional $E_{\text{kin}}[n]$.

The nonlocal effect was first incorporated into the kinetic functional E_{CAT} by Chacón, Alvarellos, and Tarazona[12] through the weighted average $\bar{n}(\mathbf{r})$ of the electron density n . The weight function was constructed so that the functional realizes the linear response of the HEG. Another type of the nonlocal kinetic functional $E_{\text{WT}}[n]$ was proposed by Wang and Teter[13], which also refers to the LRF of the HEG to formulate the integral kernel in the functional. Explicitly, the nonlocal term $E_{\text{WT}}^{\text{nlloc}}[n]$ in the WT functional is in the form

$$E_{\text{WT}}^{\text{nlloc}}[n] = C_{\text{WT}}^{\text{nlloc}} \int d\mathbf{r} d\mathbf{r}' n(\mathbf{r})^\alpha \omega_0(k_F |\mathbf{r} - \mathbf{r}'|) n(\mathbf{r}')^\alpha \quad (4)$$

where k_F is the Fermi momentum of the HEG with density n_0 and is given by $k_F = (3\pi^2 n_0)^{1/3}$. α in Eq. (4) was taken as 5/6 in the original development. For the bulk system, the average electron density in the unit cell can be adopted to n_0 . The function ω_0 is related to the LRF of the HEG and it has an oscillatory behavior in real space. It is, thus, plausible that the functional is capable of producing the quantum oscillations responsible for the creation of the shell structures in atoms. Actually, Figs. 8 and 9 in Ref. [13] show that the $E_{\text{WT}}[n]$ functional yields weak, but apparent shell structures in the density profiles of atoms. Motivated by this work, Wang, Govind, and Carter made an improvement on the WT functional in Ref. [14] and, further, developed a density-dependent kernel in Ref. [15]. However, adapting

the LRF of the HEG to atomic or molecular systems might be problematic since it is not straightforward to specify the corresponding Fermi momentum k_F for the given different positions \mathbf{r} and \mathbf{r}' since the average electron density n_0 is not well defined in contrast to the bulk systems. Along this line, Huang and Carter devised a method which incorporates the gradient of the density into the kernel for the applications to semiconductors[16]. However, even when k_F is determined somehow, there is no good reason that LRF for the HEG will be successfully applied to the systems with large inhomogeneities. It is desirable to build a novel LRF based on another reference system to construct the nonlocal kinetic energy functional suitable for the applications to atoms and molecules. Actually, there have been a lot of works besides the developments noted above to extend the applicability of OF-DFT, e.g. Mi, Genova, and Pavanello provided a sophisticated nonlocal functional by imposing some exact conditions on the kernel[17, 18]; and Constantin, Fabiano, and Sala constructed a band-gap energy dependent nonlocal term[19]. One can also find concise reviews of the recent developments in OF-DFT, for instance, in Refs. [6, 20].

In a recent work[21], a new DFT for electrons was developed on the basis of the electron distribution $n^e(\epsilon)$ on the energy coordinate ϵ . The distribution $n^e(\epsilon)$, referred to as energy electron density, is given by the projection of the density $n(\mathbf{r})$ onto the coordinate ϵ , thus,

$$n^e(\epsilon) = \int d\mathbf{r} n(\mathbf{r})\delta(\epsilon - v_{\text{def}}(\mathbf{r})) \quad (5)$$

where $v_{\text{def}}(\mathbf{r})$ is the potential introduced to define the energy coordinate and the external potential $v_{\text{ext}}(\mathbf{r})$ of interest is adopted usually. Explicitly, the coordinate ϵ is given by

$$v_{\text{def}}(\mathbf{r}) = \sum_A \frac{Z_A}{|\mathbf{r} - \mathbf{R}_A|} \quad (6)$$

where \mathbf{R}_A and Z_A are the position vector and the charge of the nucleus A, respectively. Importantly, it can be proved in parallel to the Hohenberg-Kohn theorem[22] that there exists one-to-one correspondence between certain *subsets* of the energy electron densities and the external potentials[21]. Furthermore, the Levy's constraint search method[4] can also be formulated within the DFT based on the energy electron density[21]. The introduction of the energy electron density $n^e(\epsilon)$ is motivated by the fact that it offers a natural framework to incorporate the nonlocal electron correlations which are crucial in describing the chemical

bond dissociations. The correlation is often referred to as static correlation(SC) or left-right correlation. In Ref. [21] a prototype of the SC energy functional was constructed utilizing $n^e(\epsilon)$ and a more sophisticated functional was developed in a subsequent paper[23].

In the present work, a prototype of the kinetic energy functional is developed for the applications to atoms, where a nonlocal kinetic potential is constructed on the energy coordinate. It should also be noted that the LRF of the individual atomic system instead of HEG is utilized to build the nonlocal term in contrast to the previous works. At this stage, our kinetic energy functional is only applicable to atoms. The performance is examined by computing the energies of the atoms with shifted nuclear charges. The radial electron distributions around the nucleus for the atom are also computed. The results are compared with those obtained by using the functional $E_{\text{TFW}}[n]$ in Eq. (3) and those by the KS-DFT calculation.

The organization of the paper is as follows. In Section 2, we provide the theoretical details for the construction of the nonlocal kinetic energy functional of the energy electron density, where a brief review of the LRF of the HEG is presented at first. Section 3 is devoted to describe the details of the numerical implementations and calculations. The results and discussion are presented in Section 4. The summary and the perspective are given in the last section.

2 Theory and Method

In this section, theoretical and methodological details are provided for the construction of the kinetic energy functional. In subsection 2.1, we briefly review the relation of the functional derivative of the kinetic potential with the linear-response function of the system. Then, we illustrate the projection of the nonlocal term in the kinetic energy functional onto the energy coordinate with a focus placed on its justification. In the third subsection, the explicit form of the kinetic energy functional is developed on the basis of the coupling-parameter integration. The methodology to realize the self-consistent field calculation (SCF) with the present approach is given in the last subsection.

2.1 Linear-Response Function

We first review the relationship between the kinetic potential and the linear response function(LRF) of the system of interest for later reference. We assume that an energy functional $E[n]$ of the density $n(\mathbf{r})$ is given. In the density functional framework, $E[n]$ can be further decomposed into the contributions

$$E[n] = E_{\text{kin}}[n] + E_{\text{H}}[n] + E_{xc}[n] + E_{\text{ext}}[n] \quad (7)$$

In Eq. (7), $E_{\text{H}}[n]$ is the Hartree energy due to the classical Coulomb repulsion among electrons, $E_{xc}[n]$ is the exchange-correlation energy, and E_{ext} is the interaction energy between the density n and the external potential $v_{\text{ext}}(\mathbf{r})$. At the equilibrium of the electronic state, the functional derivative of the energy with respect to the density becomes the chemical potential μ of the electron,

$$\begin{aligned} \frac{\delta E[n]}{\delta n(\mathbf{r})} &= \frac{\delta E_{\text{kin}}[n]}{\delta n(\mathbf{r})} + \frac{\delta}{\delta n(\mathbf{r})} (E_{\text{H}}[n] + E_{xc}[n] + E_{\text{ext}}[n]) \\ &= v_{\text{kin}}[n](\mathbf{r}) + v_{\text{eff}}[n](\mathbf{r}) = \mu \end{aligned} \quad (8)$$

where $v_{\text{eff}}[n](\mathbf{r})$ is the effective potential due to the electron correlations and the external potential. Since it is assumed the system is in the stationary state, the second derivative of the left hand side of Eq. (8) leads to zero,

$$\frac{\delta^2 E[n]}{\delta n(\mathbf{r})\delta n(\mathbf{r}')} = \frac{\delta v_{\text{kin}}[n](\mathbf{r})}{\delta n(\mathbf{r}')} + \frac{\delta v_{\text{eff}}[n](\mathbf{r})}{\delta n(\mathbf{r}')} = 0 \quad (9)$$

It should be noticed that the second term of the right hand side of the first equality in Eq. (9) represents the inverse of the response function $\chi(\mathbf{r}, \mathbf{r}')$ of the system. Thus, the functional derivative of the kinetic potential is directly related to the response function of the system,

$$\frac{\delta v_{\text{kin}}[n](\mathbf{r})}{\delta n(\mathbf{r}')} = -\frac{\delta v_{\text{eff}}[n](\mathbf{r})}{\delta n(\mathbf{r}')} = -\chi^{-1}(\mathbf{r}, \mathbf{r}') \quad (10)$$

This equation constitutes the basis of the constructions of the nonlocal kinetic functionals $E_{\text{CAT}}[12]$, $E_{\text{WT}}[13]$, and their modifications. Importantly, all of these studies refer to the Lindhard function[24], that is, the linear-response function $\chi_0(k_F; |\mathbf{r} - \mathbf{r}'|)$ of the homogeneous electron gas (HEG) for the sake of numerical convenience. In the construction of the

nonlocal energy in the WT functional[13], for instance, the integral kernel ω in Eq. (4) is obtained by excluding the terms corresponding to the local and semi-local energies E_{TF} and E_{vW} from $-\chi_0^{-1}$. Although the average density n_0 is well defined in bulk system, it cannot be determined for atoms and molecules at least in a natural manner. Moreover, the applicability of the LRF of the HEG to atoms and molecules that have extreme inhomogeneity is not yet well examined. It is, thus, desirable to devise a new approach using the LRF for some *inhomogeneous* reference system to construct the kinetic energy density functional applicable to the systems with large inhomogeneities.

2.2 Projection of Nonlocal Kinetic Energy Functional onto the Energy Coordinate

As mentioned in Introduction, a novel framework of the DFT was developed[21] in 2018 on the basis of the energy electron density $n^\epsilon(\epsilon)$ defined in Eq. (5). The construction of this theory was, in part, motivated by a hypothesis by Parr et al. in Ref. [25]. They advocated that the contours of the electron densities of molecules are more or less parallel to those of the bare nuclear potentials, that is, Eq. (6) itself. Actually, this is valid for the densities in atomic systems. In the molecular systems, however, the parallelism is established only approximately unless the atoms in the molecule are placed with infinite distances. The success of the local-density approximation (LDA), which constitutes the backbone of DFT, suggests the fact that the electrons at the different places with the same electron density feel roughly the same exchange and correlation energy density U_{xc} . Provided that the electron density is nearly constant on the contour surface of the energy coordinate ϵ , it is possible to consider that U_{xc} is almost constant on the surface with the coordinate ϵ . Hence, the electron density can be safely compiled into the distribution on the energy coordinate without the loss of the information contents of the electron density. Importantly, spatially nonlocal quantity can be incorporated into the functional by virtue of the projection as demonstrated in Refs. [21, 23]. With these in mind, we reformulate the nonlocal term $E_{\text{WT}}^{\text{nlc}}[n]$ in Eq. (4) with the method of the energy representation. First, we consider the general form $E_{\text{gWT}}^{\text{nlc}}[n]$ of the

nonlocal term of the WT functional, which may be written as

$$E_{\text{gWT}}^{\text{nlloc}}[n] = C_{\text{gWT}}^{\text{nlloc}} \int d\mathbf{r} d\mathbf{r}' n(\mathbf{r})^\alpha \omega(\mathbf{r}, \mathbf{r}') n(\mathbf{r}')^\alpha \quad (11)$$

Note that the integral kernel ω_0 built for the HEG is replaced by some general function ω in Eq. (11).

Let \mathcal{R}_ϵ be the spatial region having the the energy coordinate ϵ , i.e. $\mathcal{R}_\epsilon = \{\mathbf{r} \in \mathbb{R}^3 : v_{\text{def}}(\mathbf{r}) = \epsilon\}$. In other words, \mathcal{R}_ϵ constitutes a hypersurface with the energy coordinate ϵ . Obviously, it is possible for an arbitrarily given \mathbf{r} to uniquely specify the spatial region $\mathcal{R}_{\epsilon(\mathbf{r})}$ to which \mathbf{r} belongs. We assume at least approximately that the electron density $n(\mathbf{r})$ is constant on each region \mathcal{R}_ϵ , that is, $n(\mathbf{r})|_{\mathbf{r} \in \mathcal{R}_\epsilon} = \text{const.}$ ($\forall \epsilon : 0 \leq \epsilon \leq \infty$). This is just the mathematical representation of the hypothesis by Parr and Berk [25]. Note that this condition is strictly satisfied for the atomic systems. It is then possible to define the function $O^e(\epsilon)$ on the energy coordinate ϵ , thus,

$$O^e(\epsilon) := n(\mathbf{r})|_{\mathbf{r} \in \mathcal{R}_\epsilon} \quad (12)$$

In Eq. (12), it is supposed that the density $n(\mathbf{r})$ is being constant on the region \mathcal{R}_ϵ specified by $\epsilon = v_{\text{def}}(\mathbf{r})$. $n(\mathbf{r})$ can be regarded as a composite function, i.e., $n(\mathbf{r}) = O^e(v_{\text{def}}(\mathbf{r}))$. Eq. (11) can then be cast into the form of the energy representation,

$$\begin{aligned} E_{\text{gWT}}^{\text{nlloc}}[n] &= C_{\text{gWT}}^{\text{nlloc}} \int d\mathbf{r} d\mathbf{r}' n(\mathbf{r})^\alpha \omega(\mathbf{r}, \mathbf{r}') n(\mathbf{r}')^\alpha \\ &= C_{\text{gWT}}^{\text{nlloc}} \int d\epsilon d\epsilon' \int d\mathbf{r} d\mathbf{r}' \delta(\epsilon - v_{\text{def}}(\mathbf{r})) \\ &\quad \times \delta(\epsilon' - v_{\text{def}}(\mathbf{r}')) n(\mathbf{r})^\alpha \omega(\mathbf{r}, \mathbf{r}') n(\mathbf{r}')^\alpha \\ &= C_{\text{gWT}}^{\text{nlloc}} \int d\epsilon d\epsilon' O^e(\epsilon)^\alpha O^e(\epsilon')^\alpha \\ &\quad \int d\mathbf{r} d\mathbf{r}' \delta(\epsilon - v_{\text{def}}(\mathbf{r})) \delta(\epsilon' - v_{\text{def}}(\mathbf{r}')) \omega(\mathbf{r}, \mathbf{r}') \\ &= C_{\text{gWT}}^{\text{nlloc}} \int d\epsilon d\epsilon' O^e(\epsilon)^\alpha \omega^e(\epsilon, \epsilon') O^e(\epsilon')^\alpha \end{aligned} \quad (13)$$

The last equality in Eq. (13) defines the WT integral kernel $\omega^e(\epsilon, \epsilon')$ on the energy coordinate. Note that the integral kernel $\omega(\mathbf{r}, \mathbf{r}')$ in the generalized WT functional is represented with the energy coordinate in Eq. (13). It is readily recognized that the transformation from

Eq. (11) to Eq. (13) can be performed without approximations as long as the constancy of $n(\mathbf{r})$ on each \mathcal{R}_ϵ is guaranteed. In practice, however, $O^e(\epsilon)$ in Eq. (13) can be taken, for instance, as the average electron density $\tilde{n}^e(\epsilon)$ of the region \mathcal{R}_ϵ , thus,

$$O^e(\epsilon) = \tilde{n}^e(\epsilon) = \Omega(\epsilon)^{-1}n^e(\epsilon) \quad (14)$$

where $\Omega(\epsilon)$ is the volume of the region \mathcal{R}_ϵ and is given by

$$\Omega(\epsilon) = \int d\mathbf{r} \delta(\epsilon - v_{\text{def}}(\mathbf{r})) \quad (15)$$

Note that the quantity $\Omega(\epsilon)$ is independent of the density $n(\mathbf{r})$ and $\tilde{n}^e(\epsilon)$ can be regarded as a functional of $n^e(\epsilon)$. The dimension of the quantity $\tilde{n}^e(\epsilon)$ in Eq. (14) is the same as that of the electron density $n(\mathbf{r})$. Thus, the dimension of $n(\mathbf{r})^\alpha$ is not changed by the replacement of $n(\mathbf{r})$ with $\tilde{n}^e(\epsilon)$. It is readily recognized that adopting $O^e(\epsilon)$ given by Eq. (14) does not ruin the equality of Eq. (13) as long as $n(\mathbf{r})$ is constant on each \mathcal{R}_ϵ . When the constancy is not fully satisfied, however, the third equality of Eq. (13) holds only approximately at least. The validity of projecting the kernel $\omega(\mathbf{r}, \mathbf{r}')$ and the density $n(\mathbf{r})$ onto the energy coordinate is guaranteed by the framework of the DFT using the distribution $n^e(\epsilon)$ where the one-to-one correspondence is established[21] between a certain subset of $n^e(\epsilon)$ and a subset of the external potential $v^e(\epsilon)$ defined with Eq. (6). The discussion noted above is provided to interpret the present approach within the framework of the WT functional, and we note that the actual implementation in this work is based on a different theory.

It is also worth discussing the numerical advantage of taking the projection of the kernel ω . In a numerical implementation, the LRF for some reference system should be somehow inverted to obtain the kinetic potential. However, it is probably infeasible in practice to make the inversion of the response function $\chi(\mathbf{r}, \mathbf{r}')$ represented on the real space since it has six variables at each matrix element. A possible way to overcome the problem is to introduce some basis functions to represent the response function so that one can reduce the size of the matrix. However, the basis functions suitable for the expansion of χ is not known to the best of our knowledge.

We close this subsection with a brief summary. Provided that the nonlocal functional model in Eq. (11) is adequate for some applications, the functional projected onto the energy

coordinate (Eq. (13)) will also be applicable since the electron density is reasonably supposed to be nearly constant on the isosurfaces of energy coordinates. In the next subsection, we provide an explicit form of a kinetic energy functional represented on the coordinate ϵ although it cannot be used for general purposes.

2.3 Nonlocal Kinetic Energy in the Energy Representation

In this subsection we develop a kinetic energy functional represented on the energy coordinate. We note that the functional will refer to the linear-response function(LRF) of some inhomogeneous electron density. In the previous works, the nonlocal term $E_{\text{WT}}^{\text{nlloc}}[n]$ defined in Eq. (4) and its sophisticated forms were tested through several applications and their efficiencies were demonstrated to a certain extent. However, it is not known whether the same form will be as effective a functional as the functional that utilizes the LRF of an inhomogeneous system. We, thus, propose a prototype of the kinetic energy functional with another form although the applicability to general systems might be lost.

In the construction of the functional it is presumed that the corresponding kinetic potential $v_{\text{kin}}[n_0](\mathbf{r})$ and the energy $E_{\text{kin}}[n_0]$ for the given density n_0 are somehow provided from the outset. This is the major drawback of the present approach since the preparation of the reasonable $v_{\text{kin}}[n_0](\mathbf{r})$ and $E_{\text{kin}}[n_0]$ can be a difficult problem by itself. However, there have been a lot of functionals that yield better kinetic potentials and energies for the non-selfconsistent densities. The choice of the functional suitable for our functional is not a subject in the present work and it will be examined in a forthcoming issue. Anyway, for a given kinetic potential $v_{\text{kin}}[n_0](\mathbf{r})$ for the reference density n_0 , it is possible to get an approximate kinetic potential $v_{\text{kin}}[n](\mathbf{r})$ for some density n around n_0 , thus,

$$\begin{aligned} v_{\text{kin}}[n](\mathbf{r}) &= v_{\text{kin}}[n_0](\mathbf{r}) + \int d\mathbf{r}' \left. \frac{\delta v_{\text{kin}}[n](\mathbf{r})}{\delta n(\mathbf{r}')} \right|_{n=n_0} (n(\mathbf{r}') - n_0(\mathbf{r}')) \\ &= v_{\text{kin}}[n_0](\mathbf{r}) - \int d\mathbf{r}' \chi_0^{-1}(\mathbf{r}, \mathbf{r}') \delta n(\mathbf{r}') \end{aligned} \quad (16)$$

where $\delta n(\mathbf{r})$ is defined as $\delta n(\mathbf{r}) = n(\mathbf{r}) - n_0(\mathbf{r})$. In deriving the second equality of Eq. 16 we use the relation of Eq. (10). Similarly, the kinetic energy $E_{\text{kin}}[n]$ can be obtained up to

the second order of δn ,

$$\begin{aligned}
E_{\text{kin}}[n] &= E_{\text{kin}}[n_0] + \int d\mathbf{r} \left. \frac{\delta E_{\text{kin}}[n]}{\delta n(\mathbf{r})} \right|_{n=n_0} \delta n(\mathbf{r}) \\
&\quad + \frac{1}{2} \int d\mathbf{r} d\mathbf{r}' \left. \frac{\delta^2 E_{\text{kin}}[n]}{\delta n(\mathbf{r}) \delta n(\mathbf{r}')} \right|_{n=n_0} \delta n(\mathbf{r}) \delta n(\mathbf{r}') \\
&= E_{\text{kin}}[n_0] + \int d\mathbf{r} v_{\text{kin}}[n_0](\mathbf{r}) \delta n(\mathbf{r}) \\
&\quad - \frac{1}{2} \int d\mathbf{r} d\mathbf{r}' \chi_0(\mathbf{r}, \mathbf{r}')^{-1} \delta n(\mathbf{r}) \delta n(\mathbf{r}')
\end{aligned} \tag{17}$$

As a major issue in the present development, we represent the nonlocal term in Eq. (16) on the energy coordinate,

$$\begin{aligned}
v_{\text{kin}}^e[n_1](\mathbf{r}) &= v_{\text{kin}}[n_0](\mathbf{r}) \\
&\quad - \int d\epsilon' \chi_0^e(\epsilon, \epsilon')^{-1} (n_1^e(\epsilon') - n_0^e(\epsilon'))
\end{aligned} \tag{18}$$

$\chi_0^e(\epsilon, \epsilon')$ in Eq. (18) can be obtained by projecting the LRF in the real space onto the energy coordinate,

$$\chi_0^e(\epsilon, \epsilon') = \int d\mathbf{r} d\mathbf{r}' \chi_0(\mathbf{r}, \mathbf{r}') \delta(\epsilon - v(\mathbf{r})) \delta(\epsilon' - v(\mathbf{r}')) \tag{19}$$

Note that $\chi_0^e(\epsilon, \epsilon')^{-1}$ represents an element of the inverse matrix of χ_0^e . Accordingly, the kinetic energy functional $E_{\text{kin}}[n]$ in Eq. (17) is transformed to

$$\begin{aligned}
E_{\text{kin}}^e[n_1] &= E_{\text{kin}}[n_0] + \int d\mathbf{r} v_{\text{kin}}[n_0](\mathbf{r}) \delta n(\mathbf{r}) \\
&\quad - \frac{1}{2} \int d\epsilon d\epsilon' \chi_0^e(\epsilon, \epsilon')^{-1} \delta n^e(\epsilon) \delta n^e(\epsilon')
\end{aligned} \tag{20}$$

As described in Appendix A, it is possible to prove that $\chi_0^e(\epsilon, \epsilon')$ is positive semi-definite and hence, invertible through the Moore-Penrose pseudo-inverse method. The detailed discussion on the eigenvector with the null eigenvalue of the matrix is shown in Ref. [26]. Thus, only the nonlocal term in the kinetic potential is described with the energy representation. In Eq. (18) it should be noticed that the first term in the right hand side is the function of \mathbf{r} , while the second term depends on the energy coordinate ϵ . It doesn't matter, however, because the kinetic potential on a spatial coordinate \mathbf{r} can be readily obtained through the transformation $\epsilon = v_{\text{def}}(\mathbf{r})$ using Eq. (6).

2.4 Self-consistent Field Calculation for Orbital-free Density-functional Theory

There have been a lot of works devoted to expedite the self-consistent field (SCF) calculations in OF-DFT. However, in the present development we are not interested in the implementation of efficient SCF techniques. Here, we devise a minimal procedure to achieve SCF convergence in our approach. A possible improvement of the algorithm will be the subject of a forthcoming issue. We start the discussion with the variational principle for the energy functional $E[n]$. As shown in Eq. (8), the minimization of the energy $E[n]$ with respect to $n(\mathbf{r})$ under the constraint that the total number of electrons is fixed at N gives the chemical potential μ for the electrons at the stationary state. That is, the potential $v[n](\mathbf{r})$ defined by $v[n](\mathbf{r}) = \frac{\delta E[n]}{\delta n(\mathbf{r})}$ is constant irrespective of \mathbf{r} at the energy minimum. Provided that the chemical potential μ is set at 0, minimization of the functional $E[n]$ is equivalent to the solution of the nonlinear equation,

$$v[n](\mathbf{r}) = 0 \quad (21)$$

Numerically the total number of electrons in a system is merely constrained through normalization at each SCF step. Within the first-order variation of n , the solution \bar{n} of the equation satisfies the following approximation

$$v[\bar{n}](\mathbf{r}) \cong v[n](\mathbf{r}) + \int d\mathbf{r}' \frac{\delta v[n](\mathbf{r})}{\delta n(\mathbf{r}')} (\bar{n}(\mathbf{r}') - n(\mathbf{r}')) = 0 \quad (22)$$

where n is an arbitrary density reasonably close to \bar{n} . Then, the formal solution for the above equation is given by

$$\bar{n}(\mathbf{r}) \cong n(\mathbf{r}) - \int d\mathbf{r}' \frac{\delta n(\mathbf{r})}{\delta v[n](\mathbf{r}')} v[n](\mathbf{r}') \quad (23)$$

Thus, the electron density n_i at the i th SCF step can be updated as

$$n_{i+1}(\mathbf{r}) = n_i(\mathbf{r}) - \int d\mathbf{r}' \frac{\delta n_i(\mathbf{r})}{\delta v[n_i](\mathbf{r}')} v[n_i](\mathbf{r}') \quad (24)$$

Unfortunately, the SCF iteration through Eq. (24) is practically infeasible because the functional derivative of the density with respect to the potential $v[n](\mathbf{r}) (= v_{\text{kin}} + v_{\text{eff}})$ cannot be readily obtained. A simple but inefficient way to bypass the calculation of the integral

kernel in Eq. (24) is to replace the kernel with a unit matrix multiplied by a small positive factor η . In our preliminary calculations, however, it was found that such an approach gives rise to quite slow convergence in the density. In the present implementation, we replace the kernel with the derivative of the density with respect to the kinetic potential, thus,

$$n_{i+1}(\mathbf{r}) = n_i(\mathbf{r}) - \eta \int d\mathbf{r}' \frac{\delta n_i(\mathbf{r})}{\delta v_{\text{kin}}[n_i](\mathbf{r}')} v[n_i](\mathbf{r}') \quad (25)$$

It is important to note that the replacement of the kernel doesn't change the stationary condition. Actually, at the convergence of the density, that is, $n_{i+1}(\mathbf{r}) - n_i(\mathbf{r}) \cong 0$, we have,

$$\int d\mathbf{r}' \frac{\delta n_i(\mathbf{r})}{\delta v_{\text{kin}}[n_i](\mathbf{r}')} v[n_i](\mathbf{r}') \cong 0 \quad (26)$$

Then, $v[n_i](\mathbf{r}') \cong 0$ is guaranteed since the kernel $\frac{\delta n_i(\mathbf{r})}{\delta v_{\text{kin}}[n_i](\mathbf{r}')}$ is always positive semidefinite and invertible. Further, we assume that the kernel in Eq. (25) is evaluated for the reference system and represented on the energy coordinate,

$$n_{i+1}(\mathbf{r}) = n_i(\mathbf{r}) + \eta \int d\epsilon' \chi_0^\epsilon(\epsilon, \epsilon') v[n_i](\epsilon') \quad (27)$$

where the potential $v[n](\epsilon)$ is defined as

$$v[n](\epsilon) = \int d\mathbf{r} \delta(\epsilon - v_{\text{def}}(\mathbf{r})) v[n](\mathbf{r}) \quad (28)$$

In Eq. (27) it is possible that the kernel $\chi_0^\epsilon(\epsilon, \epsilon')$ plays as a nonlocal weight function acting on the potential to expedite the SCF. The choice of the value η will affect more or less the rate of the SCF convergence and accuracy of the results. In the present work, the appropriate value of η is determined empirically as $\eta = 0.05$, and it is used in the SCF calculations throughout.

Finally, we describe a minor issue for the density in the SCF iteration. It is common to employ the variable $\varphi(\mathbf{r})$, that is, the square root of the density $n(\mathbf{r})$,

$$\varphi(\mathbf{r}) = n(\mathbf{r})^{\frac{1}{2}} \quad (29)$$

to avoid the situation that $n(\mathbf{r})$ becomes negative during the SCF. Then, the SCF iteration using Eq. (25) should be modified as

$$\varphi_{i+1}(\mathbf{r}) = \varphi_i(\mathbf{r}) - \eta \int d\mathbf{r}' \left\{ \frac{\delta \varphi(\mathbf{r})}{\delta n(\mathbf{r})} \frac{\delta n(\mathbf{r})}{\delta v_{\text{kin}}[n](\mathbf{r}')}\right\}_{n_i} v[n_i](\mathbf{r}') \quad (30)$$

Accordingly, Eq. (27) is rewritten as

$$\varphi_{i+1}(\mathbf{r}) = \varphi_i(\mathbf{r}) + \eta \int d\epsilon' \tilde{\chi}_0^e(\epsilon, \epsilon') v[n_i](\epsilon') \quad (31)$$

where $\tilde{\chi}_0^e$ is defined as

$$\begin{aligned} \tilde{\chi}_0^e(\epsilon, \epsilon') = \int d\mathbf{r} d\mathbf{r}' \left\{ \frac{\delta\varphi(\mathbf{r})}{\delta n(\mathbf{r})} \frac{\delta n(\mathbf{r})}{\delta v_{\text{kin}}(\mathbf{r}')} \right\}_{n_0} \\ \times \delta(\epsilon - v_{\text{def}}(\mathbf{r})) \delta(\epsilon' - v_{\text{def}}(\mathbf{r}')) \end{aligned} \quad (32)$$

In Eq. (32), n_0 is the density of the reference system.

3 Computational Details

As a benchmark test we apply the kinetic energy functional of Eq. (20) to pseudo atomic systems(H, He, Ne, and Ar), where the core charge Z_v of each atom is shifted by q within the range of $-0.2 \leq q \leq +0.2$ in the unit of the elementary charge. Throughout the calculations, the system with $q = 0$ is taken as the reference system to build the response function $\chi_0^e(\epsilon, \epsilon')$ as well as the density $n_0^e(\epsilon)$ on the energy coordinate. Then, the variation of the kinetic energy of each atom is compared with that given by the Kohn-Sham DFT calculation. We also employ other OF-DFT functionals, that is, $E_{\text{TF}}[n]$ in Eq. (1) and $E_{\text{TFW}}[n]$ in Eq. (3) for comparisons. In these calculations the electron density $n(\mathbf{r})$ is individually optimized beforehand in the separate Kohn-Sham DFT calculation.

Next, we perform the variational calculation using the kinetic potential $v_{\text{kin}}^e[n](\mathbf{r})$ in Eq. (18) to obtain the self-consistent electron density, where the reference density $n_0(\mathbf{r})$ is employed as an initial guess. Then, we compute the radial distribution functions $4\pi r^2 n(r)$ of the Ne and Ar systems with $q = 0.2$ through OF-DFT SCF calculations using Eq. (31).

The first subsection provides the details of the base program to perform numerical OF-DFT calculations using the real-space grids. In the second subsection, we introduce the construction of the pseudo atoms that mimic H, He, Ne, and Ar, where the bare Coulomb potentials are replaced by some local pseudopotentials to realize the smooth behaviors of the densities near the atomic cores although the properties of the corresponding atoms are no longer maintained. The numerical details for the construction of the response function and

the energy electron density on the energy coordinate is described in the third subsection. A numerical issue, which arises in the inversion of the response function, will be addressed in the fourth subsection. The last subsection provides the numerical recipes for the extension of the present approach to a system with a covalent bond.

3.1 Real-space Grid Approach

The program module for the present OF-DFT is newly developed and embedded in the Kohn-Sham DFT program ‘Vmol’[27–32] based on the real-space grid approach[33, 34]. Thus, the electron density $n(\mathbf{r})$ is represented on the real-space grids uniformly placed within a cubic box. Throughout the present calculations, the size of the real-space cell is set at $L = 18.354$ a.u. and each axis is discretized by equally spaced 64 grids, which leads the grid width $h = 0.2868$ a.u. The exchange-correlation energy $E_{xc}[n]$ in Eq. (7) is evaluated with the BLYP functional[35, 36]. To make comparisons among the kinetic energy functionals, we also employ the functionals $E_{TF}[n]$ and $E_{vW}[n]$ given in Eqs. (1) and (2), respectively. The Laplacian in Eq. (2) is represented with the fourth-order finite difference method[33, 34].

3.2 Construction of Pseudo Atoms

To achieve the OF-DFT calculation within the plane-wave or real-space grid approach, it is also a subject of critical importance to develop *local* pseudopotentials for atoms. Unfortunately, to the best of our knowledge, there have not been sufficient amount of works along this line. In the present study, however, we are not interested in the applications to realistic atoms. We, thus, consider ‘pseudo’ atoms which stem from Hydrogen, Helium, Neon, and Argon atoms. The sole purpose of the pseudization is to realize the smooth variation of the density so that the real-space grid approach can adequately describe it. To this end we merely adopt the local term $V_{\text{loc}}(r)$ in an existing pseudopotential set as a function of the distance r between the electron and the nucleus. As a specific treatment for pseudo Ne and Ar atoms, we additionally embed the potential $\Delta V_s(r)$ assigned as the S component in the nonlocal term to mimic the repulsive potential due to the core electrons. Actually, we found that the valence electrons in Ne and Ar erroneously penetrate into the core region without

the term $\Delta V_s(r)$. In the present calculation, we use the terms in the BHS pseudopotential[37] as components to build the potential. We summarize the form of the local pseudopotential $V_{\text{ps}}^{\text{A}}(r)$ for atom A(= H, He, Ne, or Ar) used in our calculations,

$$\left\{ \begin{array}{l} V_{\text{ps}}^{\text{A}}(r) = V_{\text{loc}}^{\text{A}}(r) \quad (\text{A} = \text{H}, \text{He}) \\ V_{\text{ps}}^{\text{A}}(r) = V_{\text{loc}}^{\text{A}}(r) + \Delta V_s^{\text{A}}(r) \quad (\text{A} = \text{Ne}, \text{Ar}) \end{array} \right. \quad (33)$$

where $V_{\text{loc}}^{\text{A}}(r)$ and $\Delta V_s^{\text{A}}(r)$ are, respectively, given in the forms,

$$V_{\text{loc}}(r) = -\frac{Z_v}{r} \left[\sum_{i=1}^2 c_i \operatorname{erf} \left[(\alpha_i)^{1/2} r \right] \right] \quad (34)$$

and

$$\Delta V_s(r) = \sum_{i=1}^3 (P_i + r^2 P_{i+3}) \exp(-\alpha_i r^2) \quad (35)$$

In Eqs. (34) and (35) we omit the superscript A for simplicity. In Eq. (34) Z_v is the corresponding valence charge for atom A. Z_v are 1.0 and 2.0 for H and He atoms, respectively, while $Z_v = 8.0$ for Ne and Ar. The coefficients c_i and α_i in Eq. (34) are tabulated in Ref. [37] for various atoms. The two sets of coefficients P_i and P_{i+3} in Eq. (35) correspond to the exponents α_i ($i = 1, 2, 3$). The set of P_i can be obtained by the numerical reconstruction of the data in Table IV in Ref. [37]. We refer the readers to the paper for the detail of the algorithm. The local pseudopotentials employed in the present calculations are displayed in Fig. 1. In the graphs for Ne and Ar atoms, it is shown that each $V_{\text{ps}}(r)$ rises notably near the core region due to the repulsive potential $\Delta V_s(r)$. It should be stressed that the pseudopotentials given in Eq. (33) are *not* optimized to reproduce the properties of the corresponding realistic atoms. Hence, the eigenvalues provided by the Kohn-Sham DFT calculation are not coincident with those constructed by the full set of pseudopotential that includes the nonlocal terms. However, it makes complete sense to compare the result given by OF-DFT with that given by the KS-DFT calculation. The time-saving double-grid technique[38] is employed to describe adequately the steep variation of the local pseudopotentials in the core region, where the width of the dense grid is set at $h/5$ throughout the calculations.

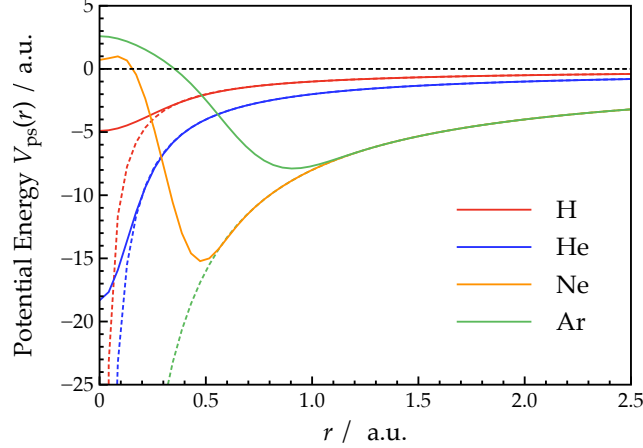


Figure 1: The local pseudopotentials constructed using Eq. (33) for H, He, Ne, and Ar pseudo atoms. The broken lines are the corresponding Coulomb potentials of the valence charges Z_v .

3.3 Energy Coordinate and Linear-response Function

As shown in Eq. (6) the bare Coulomb potential is usually employed as the defining potential $v_{\text{def}}(\mathbf{r})$ for the energy coordinate ϵ . However, another potential $v'_{\text{def}}(\mathbf{r})$ can also be adopted as a defining potential as long as the relation $v'_{\text{def}}(\mathbf{r}_A) = v'_{\text{def}}(\mathbf{r}_B)$ holds for any points \mathbf{r}_A and \mathbf{r}_B satisfying $v_{\text{def}}(\mathbf{r}_A) = v_{\text{def}}(\mathbf{r}_B)$ [21]. In the present development, in contrast to the previous works[21, 23], we employ the opposite sign of the BHS local potential $V_{\text{loc}}^{\text{BHS}}(r)$ as the defining potential, i.e., $v_{\text{def}}(\mathbf{r}) = -V_{\text{loc}}^{\text{BHS}}(r)$.

The log-scaled energy coordinate with the range of $(\log \epsilon_{\text{min}}, \log \epsilon_{\text{max}})$ is uniformly discretized by N_{grid}^e grid points. Then, the energy electron density $n^e(\epsilon)$ in Eq. (5) and the response function $\chi_0^e(\epsilon, \epsilon')$ in Eq. (19) are numerically constructed on the discrete energy coordinates. The parameters N_{grid}^e and $(\epsilon_{\text{min}}, \epsilon_{\text{max}})$ are individually determined for each atom and the values are summarized in the ‘Supplementary Material’.

The linear-response function(LRF) $\chi_0(\mathbf{r}, \mathbf{r}')$ in Eq. (19) for a reference system is obtained by the 2nd-order perturbation theory. To do this, we first solve a Kohn-Sham equation for the reference system(i.e., $q = 0.0$),

$$\left(-\frac{1}{2}\nabla^2 + v_{\text{eff}}[n_0](\mathbf{r}) \right) \varphi_i^0(\mathbf{r}) = \epsilon_i^0 \varphi_i^0(\mathbf{r}) \quad (36)$$

where n_0 is the electron density constructed from the self-consistent solutions $\{\varphi_i^0\}$, and $\{\epsilon_i^0\}$

is the corresponding eigenvalues. Then, the LRF is evaluated as

$$\chi_0(\mathbf{r}, \mathbf{r}') = \sum_i^{\text{occ}} \sum_a^{\text{vir}} \frac{1}{\epsilon_a^0 - \epsilon_i^0} \varphi_i^{0*}(\mathbf{r}) \varphi_a^0(\mathbf{r}) \times \varphi_a^{0*}(\mathbf{r}') \varphi_i^0(\mathbf{r}') \quad (37)$$

where the indices i and a are for the occupied and virtual orbitals, respectively. The LRF $\chi_0^e(\epsilon, \epsilon')$ defined on the energy coordinate is merely obtained by the projection,

$$\chi_0^e(\epsilon, \epsilon') = \int d\mathbf{r} d\mathbf{r}' \delta(\epsilon - v_{\text{def}}(\mathbf{r})) \delta(\epsilon' - v_{\text{def}}(\mathbf{r}')) \chi_0(\mathbf{r}, \mathbf{r}') \quad (38)$$

Explicitly, the numbers of the virtual orbitals included in Eq. (37) are 23 for H and He, 20 for Ne, and 22 for Ar. It is found that the LRF is rather insensitive to the number of the virtual orbitals. However, attention should be paid to the upper limit since the virtual orbitals with larger eigenvalues can not be adequately accommodated in the real-space cell.

Note that the kinetic potential $v_{\text{kin}}[n_0](\mathbf{r})$ in Eq. (18) as well as $E_{\text{kin}}[n_0]$ in Eq. (20) for the reference system can also be obtained from the solution of Eq. (36). Specifically for $v_{\text{kin}}[n_0](\mathbf{r})$, we use the relation,

$$v_{\text{kin}}[n_0](\mathbf{r}) = -v_{\text{eff}}[n_0](\mathbf{r}) \quad (39)$$

Although the response function $\chi_0(\mathbf{r}, \mathbf{r}')$ can be easily computed, the projection onto the energy coordinate through Eq. (19) is rather time-consuming. This could be a serious problem when we consider its applications to larger systems in a later development. In our perspective, however, the LRF of a composite system might be adequately constructed from the overlap of the LRF of the constituent systems on the energy coordinate.

3.4 Inverse of Linear-response Function

We also make a remark on the inversion of the LRF defined on the energy coordinate. As shown in Appendix A, the matrix $\chi_0^e(\epsilon, \epsilon')$ is positive semi-definite, and hence can be inverted using the pseudo-inverse method. Here, we discuss another issue associated with the inversion. Suppose that the matrix is given in the form of the spectral decomposition,

$$\chi_0^e(\epsilon, \epsilon') = \sum_i^{N_{\text{grid}}^e} \langle \epsilon | \gamma_i \rangle g_i \langle \gamma_i | \epsilon' \rangle \quad (40)$$

where $\gamma_i(\epsilon)$ is the eigenvector of the matrix χ_0^e , and g_i is the corresponding eigenvalue. The matrix includes at least one null eigenvector with the 0 eigenvalue due to the condition that the number of electrons is being fixed. However, it is found unexpectedly that there exists a lot of eigenvectors with substantially zero eigenvalues for the atomic systems studied in the present work. In addition, it is also revealed that the eigenvector with the largest eigenvalue dominates the construction of the matrix. Shown in Fig. 2(a) is the eigenvalues $\{g_i\}$ plotted

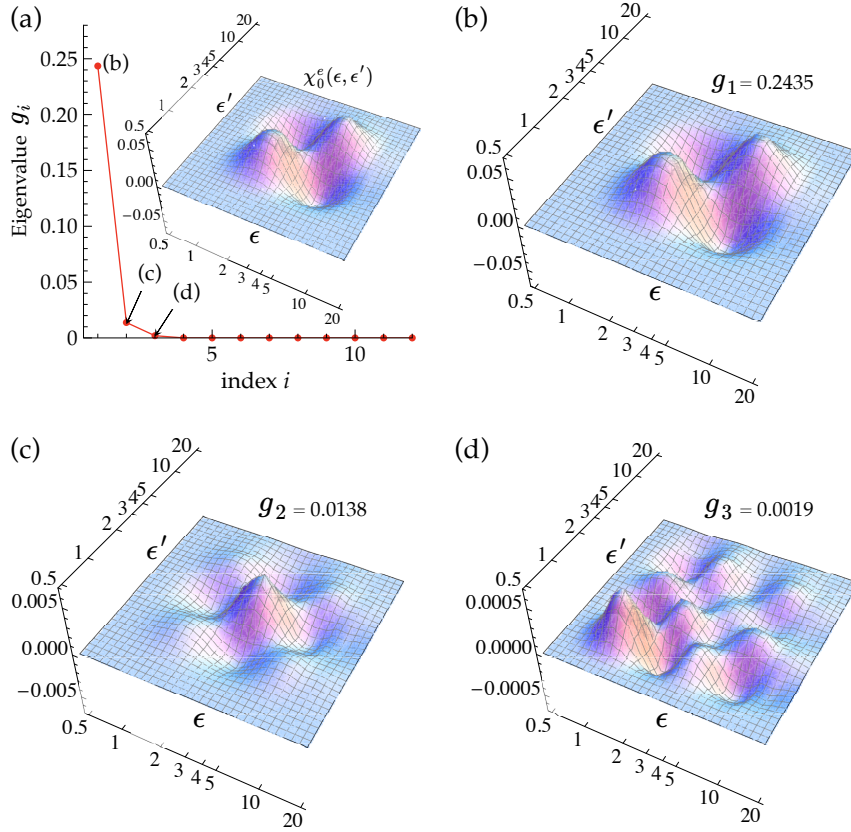


Figure 2: (a) The plot of the eigenvalues $\{g_i\}$ in descending order for the pseudo Ar atom. The linear-response function $\chi_0^e(\epsilon, \epsilon')$ of the Ar atom is superposed. (b), (c), and (d) show the functions $g_i \gamma_i(\epsilon) \gamma_i(\epsilon')$ (see Eq. (40)) for the indices $i = 1, 2$, and 3 , respectively. Units of the energy coordinate ϵ is a.u., while that of $\chi_0^e(\epsilon, \epsilon')$ is a.u.⁻².

for the pseudo Ar atom in descending order, where the three-dimensional graph for the LRF $\chi_0^e(\epsilon, \epsilon')$ is also superposed. The notations (b), (c), and (d) in the plot denote the three largest eigenvalues, for which the corresponding LRF components $g_i \gamma_i(\epsilon) \gamma_i(\epsilon')$ are drawn in Figs. 2(b), 2(c) and 2(d), respectively. By consulting Figs. 2(a) and 2(b), it is recognized that

the eigenvector γ_1 with the lowest frequency is dominant in the decomposition of the total LRF in Eq. (40). It seems that higher frequency mode γ_i gives much smaller contribution to the LRF as observed in the sequence of Figs. 2(b), 2(c) and 2(d). It is remarkable that the response function generated by the lowest frequency mode γ_1 faithfully realizes the total LRF shown in Fig. 2(a). It is found that this trend is common to all the atoms treated in the present work. In the pseudo-inverse approach, the inverse of the LRF of Eq. (40) can be obtained by

$$\chi_0^e(\epsilon, \epsilon')^{-1} = \sum_i^{N_{\text{grid}}^e - 1} \langle \epsilon | \gamma_i \rangle g_i^{-1} \langle \gamma_i | \epsilon' \rangle \quad (41)$$

Note that the eigenvector with 0 eigenvalue is to be excluded from the summation in the right hand side of Eq. (41). In a practical calculation, however, the smallest eigenvalue may not become exactly zero due to the numerical error. Thus, the eigenvector with the smallest eigenvalue should be excluded from the construction of the inverse matrix. However, it is found in the preliminary calculations that the faithful execution of Eq. (41) gives rise to the unphysical oscillations in the matrix $\chi_0^e(\epsilon, \epsilon')^{-1}$ due to the high frequency modes multiplied by the huge values g_i^{-1} . Actually, as demonstrated in Appendix B, the magnitude of the component of the response function $\chi_0^e(\epsilon, \epsilon')$ with a small eigenvalue is found to be within the grid error due to the use of the real-space grids in representing the function $\chi_0(\mathbf{r}, \mathbf{r}')$. Thus, the summation in Eq. (41) should be truncated after the first few leading terms in practice. Throughout this work, we only consider the eigenvector γ_1 with the largest eigenvalue g_1 to construct the inverse of the LRF. The effect of the inclusion of the residual contributions will be examined later.

3.5 Extension to Molecular System

As a pilot test, we apply the present approach to the calculation of the potential energy curve of the covalent bond of an H_2 molecule. For this purpose, the LRF for the molecule has to be constructed. To make the computational cost to increase linearly with the system size, it is necessary to build the LRF using those for the constituent atoms as building blocks. In the following, we provide an instantaneous and straightforward approximation as a prototype to realize such a construction. We stress that other elaborate approaches might be potentially

developed to improve the nonlocal functional. Anyway, we suppose that a hydrogen molecule comprises hydrogen atoms H_A and H_B placed at \mathbf{R}_A and \mathbf{R}_B , respectively, with a certain distance $R = |\mathbf{R}_A - \mathbf{R}_B|$. Then it is assumed that two LRFs $\chi_0^A(\mathbf{r}, \mathbf{r}')$ and $\chi_0^B(\mathbf{r}, \mathbf{r}')$ are obtained through Eq. (37) for the isolated hydrogen atoms H_A and H_B , respectively. Here we approximate that the LRF of the whole system is merely given by the sum of these atomic LRFs, thus,

$$\chi_0(\mathbf{r}, \mathbf{r}') = \chi_0^A(\mathbf{r}, \mathbf{r}') + \chi_0^B(\mathbf{r}, \mathbf{r}') \quad (42)$$

Accordingly, the corresponding LRF $\chi_0^e(\epsilon, \epsilon')$ of the molecule defined on the energy coordinate is provided by the sum of the projections of the LRFs of the individual atoms,

$$\chi_0^e(\epsilon, \epsilon') = \chi_0^A(\epsilon, \epsilon') + \chi_0^B(\epsilon, \epsilon') \quad (43)$$

It is readily recognized that the LRF $\chi_0^e(\epsilon, \epsilon')$ is also positive semi-definite and invertible. The projection of each atomic LRF can be, of course, performed through Eq. (38), where the defining potential v_{def} is constructed for the molecular system with the given interatomic distance R . The method to project the individual LRFs onto those defined on the energy coordinate is the same as noted in subsection 3.3. The detailed assessment of the accuracy and property of Eq. (43) will be an issue in the future works.

The reference electron density $n_0(\mathbf{r})$ is also provided by the sum of the individual electron densities $n_0^A(\mathbf{r})$ and $n_0^B(\mathbf{r})$, respectively, for H_A and H_B , thus,

$$n_0(\mathbf{r}) = n_0^A(\mathbf{r}) + n_0^B(\mathbf{r}) \quad (44)$$

Lastly, we have to determine the corresponding reference kinetic energy $E_{\text{kin}}[n_0]$ in Eq. (17) and potential $v_{\text{kin}}[n_0](\mathbf{r})$ in Eq. (18). Since H_2 is a closed two electrons system, the exact kinetic energy and potential can be provided for an arbitrarily given electron density. Explicitly, for the density n_0 they are merely given by

$$E_{\text{kin}}[n_0] = \int d\mathbf{r} n_0(\mathbf{r})^{\frac{1}{2}} \left(-\frac{1}{2} \nabla^2 \right) n_0(\mathbf{r})^{\frac{1}{2}} \quad (45)$$

$$v_{\text{kin}}[n_0](\mathbf{r}) = n_0(\mathbf{r})^{-\frac{1}{2}} \left(-\frac{1}{2} \nabla^2 \right) n_0(\mathbf{r})^{\frac{1}{2}} \quad (46)$$

It will also be helpful to make a brief comment on the method applicable to the systems with many electrons for future implementations although not used in the present work.

Suppose that a system consists of two subsystems A and B of which electronic structures are individually obtained. When these subsystems are infinitely separated, $E_{\text{kin}}[n_0]$ and $v_{\text{kin}}[n_0](\mathbf{r})$ are exactly given by the sum of the kinetic energies and potentials of the individual subsystems. At the finite separation, however, one should introduce the bifunctionals, that is, the non-additive kinetic energy $E_{\text{kin}}^{\text{nad}}[n_0^{\text{A}}, n_0^{\text{B}}]$ and the potential $v_{\text{kin}}^{\text{nad}}[n_0^{\text{A}}, n_0^{\text{B}}](\mathbf{r})$, which are, respectively, defined as

$$E_{\text{kin}}^{\text{nad}}[n_0^{\text{A}}, n_0^{\text{B}}] = E_{\text{kin}}[n_0] - (E_{\text{kin}}[n_0^{\text{A}}] + E_{\text{kin}}[n_0^{\text{B}}]) \quad (47)$$

$$v_{\text{kin}}^{\text{nad}}[n_0^{\text{A}}, n_0^{\text{B}}](\mathbf{r}) = v_{\text{kin}}[n_0](\mathbf{r}) - (v_{\text{kin}}[n_0^{\text{A}}](\mathbf{r}) + v_{\text{kin}}[n_0^{\text{B}}](\mathbf{r})) \quad (48)$$

Then, the summation of the kinetic energies or potentials of the subsystems are corrected by adding these non-additive terms. In practice, one has to evaluate Eqs. (47) and (48) approximately by means of some kinetic GGA functional. Originally, the non-additive term has a major relevance to the implementation of the frozen-density embedding theory (FDET)[39]. Actually, there has been a lot of developments and discussions in this context[6, 39–42]. In the present study, however, we focus our interest on the performance of our nonlocal kinetic energy functional on the energy coordinate, and we do not consider the application of Eqs. (47) and (48).

In the computation of the potential energy curve for H_2 molecule, the electron density of the molecule as well as the reference system are optimized by the Kohn-Sham DFT with the method shown in subsection 3.1. For the electron-nuclear potential of the H_2 molecule, the nonlocal part in the pseudopotential is also included in contrast to the calculation of the H atom in order to ensure the formation of the sound chemical bond. Explicitly, the nonlocal pseudopotential in the form developed by Kleinman and Bylander[43] is included besides the local term in Eq. (33).

We also perform an additional interesting calculation to examine the effect of the variation of the LRF $\chi_0^e(\epsilon, \epsilon')$ on the potential energy curve of H_2 . To do this, the LRF is constructed from the wave functions of an electron bound to a 3-dimensional harmonic potential $U_{\text{HP}}(r) = \frac{1}{2}kr^2$ where k is the spring constant and r is the radial distance of the electron from the center. The center of the harmonic potential is placed at each nucleus. Thus, the component LRFs in Eq. (42) are each constructed from the wave functions for the harmonic potential $U_{\text{HP}}(r)$

instead of the pseudopotential of the H atom. The spring constant k is chosen so that the Gaussian obtained as the ground state wave function for U_{HP} maximally fits the 1s orbital of H atom. The exponent of the normalized Gaussian can be obtained as 0.270950 through least-square fitting as provided in Ref. [44]. The corresponding value of k is evaluated as 0.294 a.u. The wave function $R_{n,l}(r)$ dependent on the principal quantum number n and the momentum quantum number l along the radial direction is analytically given as a solution for the Kummer's differential equation[45]. Explicitly, we consider up to 4s orbital with $l = 0$ and p_x orbital with $(n, l) = (0, 1)$ in the construction of the LRF. The radial wave function $R_{n,l}(r)$ is then multiplied by the spherical harmonics to provide the total wave function. The LRF for the electron in the harmonic potential is constructed through the perturbation theory.

4 Results and Discussion

First, we apply our kinetic energy functional $E_{\text{kin}}^e[n]$ to the pseudo atoms (H, He, Ne, and Ar) to compute the variation of the kinetic energy for each atom when the valence charge Z_v is shifted by q within the range of $-0.2 \leq q \leq 0.2$ in the unit of the elementary charge. The density $n(\mathbf{r})$ optimized by Kohn-Sham DFT (KS-DFT) is adopted as the argument of the functional. Next, the self-consistent densities for the Ne and Ar atoms are computed through the present OF-DFT approach. The radial distributions of the electrons are compared with those obtained by the KS-DFT calculations. To examine the applicability to a molecular system, the method is applied to the computation of the covalent bond in a hydrogen molecule chosen as a pilot system, where the validity of the representation of the response function on the energy coordinate is also discussed.

4.1 Kinetic Energy Calculation Using Non-self-consistent Density

Figure 3 shows the profile of the kinetic energy $E_{\text{kin}}^e[n]$ (Eq. (20)) with respect to the variation of the valence charge Z_v ($0.8 \leq Z_v \leq 1.2$) of the pseudo H atom. To make comparisons we also employ the Thomas-Fermi (TF) functional E_{TF} in Eq. (1) and E_{TF} combined with the Weizsäcker correction, that is, the TFW functional E_{TFW} in Eq. (3). The

electron density $n(\mathbf{r})$ adopted as the argument is that optimized through the self-consistent field (SCF) calculation of the KS-DFT method. In every plot, the kinetic energy increases monotonically with respect to the increase in the valence charge Z_v . The increase in Z_v causes the stabilization of the potential energy of the system, which leads to the increase in the kinetic energy. As observed in the figure, the functional $E_{\text{kin}}^e[n]$ developed in the present work shows excellent agreement with the result of KS-DFT except for the region around $Z_v = 0.80$. Although the kinetic energy at $Z_v = 0.80$ varies by ~ 0.13 a.u. from that of the reference system with $Z_v = 1.0$, the deviation of the present work from the KS-DFT value stays ~ 0.01 a.u. It is notable that the present work perfectly realizes the KS-DFT values around another end of the valence charge, i.e., $Z_v = 1.2$. It is observed in the figure that

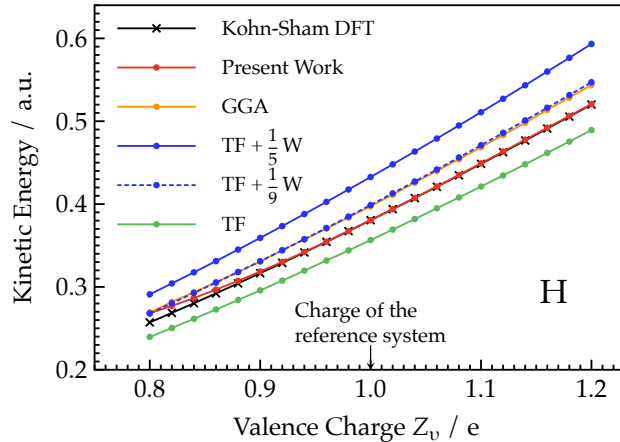


Figure 3: Plots of the kinetic energies computed by various kinetic functionals for the variation of the valence charge Z_v of the pseudo H atom. The atom with $Z_v = 1.0$ is taken as the reference system. The value of the ‘Present Work’ is provided using Eq. (20). The GGA functional is that given in Eq. (49) or equivalently Eq. (12) in Ref. [46]. ‘TF + 1/5W’ and ‘TF + 1/9W’ are obtained by Eq. (3) with $\lambda = 1/5$ and $1/9$, respectively. ‘TF’ is evaluated by Eq. (1).

the energy of the TF functional is always lower than that of KS-DFT, where the difference between the TF and the KS-DFT energy is ~ 0.03 a.u. at the most. Unfortunately, it is found that the inclusion of the Weizsäcker term with the factor $\lambda = \frac{1}{5}$ overcorrects the underestimation of the TF functional. Adopting the factor $\lambda = \frac{1}{9}$, which correctly reproduces the LRF of the homogeneous electron gas in the small \mathbf{k} region, provides much better result.

The fact that TFW functional with $\lambda = \frac{1}{9}$ is superior to $\lambda = \frac{1}{5}$ is somewhat surprising because it was demonstrated in Ref. [11] that the choice of $\lambda = \frac{1}{5}$ gives the smallest errors in the evaluation of the total energies of various atoms. It is possible that the result is affected by the smooth behavior of the density due to the pseudization of the atom. We also examine the performance of a sophisticated GGA (generalized gradient approximation) functional for the kinetic energy. Explicitly, we employ Eq. (12) in Ref. [46], which was heuristically developed by integrating the several types of the GGA functionals to minimize the error for the kinetic energies of the 77 molecules. The explicit form of the functional for a spin is given by

$$E_{\text{kin}}^{\text{GGA}}[n] = 2^{\frac{2}{3}} C_{\text{TF}} \int d\mathbf{r} n(\mathbf{r})^{\frac{5}{3}} \times \left(1 + \frac{A_1 x^2}{1 + A_2 x \sinh^{-1} x} - \frac{A_3 x}{1 + A_4 x} \right) \quad (49)$$

where x represents the inhomogeneity of the density of the spin and defined by $|\nabla n(\mathbf{r})|/n(\mathbf{r})^{\frac{4}{3}}$. The parameters $\{A_i\}$ in Eq. (49) are specified as $A_1 = 0.0055$, $A_2 = 0.0253$, $A_3 = 0.072$, and $A_4 = 2^{\frac{5}{3}}$. Despite the sophistication of the GGA functional, it offers quite minor improvement on the TFW functional with $\lambda = \frac{1}{9}$ as shown in the figure.

Here, we discuss the contribution of the nonlocal term in Eq. (20). As shown in the equation, the nonlocal energy is the quantity proportional to the 2nd order of the deviation of the energy electron density $\delta n^e(\epsilon) = n^e(\epsilon) - n_0^e(\epsilon)$. Thus, the contribution is zero at $Z_v = 1.0$ in principle and considered to be larger at the both ends of the plot. Actually, the third term in Eq. (20) amounts to 0.024 a.u. and 0.013 a.u., respectively, at $Z_v = 0.8$ and 1.2, although the contributions are much smaller as compared with those of the local term. For the calculation of Fig. 3, the energy coordinate ϵ ($0.05 \leq \epsilon \leq 5.0$) in the unit of a.u. is discretized by $N_{\text{grid}}^e = 25$ grids as listed in the ‘Supplemental Material’. We examine the numerical robustness by setting $N_{\text{grid}}^e = 15$ in an additional calculation. It is demonstrated that the nonlocal terms become 0.025 a.u. at $Z_v = 0.8$, and 0.014 a.u. at $Z_v = 1.2$, which shows the numerical stability of the functional with respect to the choice of the width of the grid.

We also examine the effect of the inclusion of the higher frequency modes in the decomposition of Eq. (40). As was described at the end of Subsec. 3.4., only the term with the

largest eigenvalue ($g_1 = 0.103$) is incorporated in the calculation of Fig. 3. It is found that considering up to the term with the secondary largest eigenvalue ($g_2 = 0.016$) leads to the deviation of the kinetic energy upward by 0.01 a.u. at $Z_v = 1.2$. Furthermore, it is also revealed that including up to the third term ($g_3 = 0.00062$) worsens the kinetic energy by 0.052 a.u. Thus, the inclusion of the residual modes besides the leading term in Eq. (40) is found to degrade the functional $E_{\text{kin}}^e[n]$. This trend also applies to the other end of the Z_v axis. At this stage, unfortunately, we have no good reason to justify the truncation in the decomposition. However, it is speculated that some statistical noise is present in the numerical construction of the LRF due to the lack of samplings, which may cause the creation of unphysical high frequency modes in $\chi_0^e(\epsilon, \epsilon')$. Actually, in our real-space grid approach, the construction of the LRF on the energy coordinate is numerically performed by projecting the data on the 64^3 grid points in the real-space cell onto the 25 grids for the energy coordinate. Seemingly, the amount of the data assigned to an energy coordinate ϵ is not sufficient when the coordinate corresponds to the atomic core region in particular. To increase the sampling points, one may consider to apply the double-grid technique[38] to the core region. We found, however, that the straightforward implementation of the method leads to the destruction of the crucial condition that the matrix $\chi_0^e(\epsilon, \epsilon')$ is positive semi-definite. In the following, we provide the results for the remaining pseudo atoms, i.e., He, Ne, and Ar.

In Fig. 4 the profiles of the kinetic energies for the pseudo He atom are presented. The energy range of the plots is extended by about 3 times as compared with that for H atom because the depth of the local pseudopotential for He is much deeper than that for H as shown in Fig. 1 and the number of electrons is twice that of H. It is clearly recognized in the figure that the plots have quite similar trend as those for the pseudo H atom. It is striking that the kinetic energy given by Eq. (20) excellently agrees with that by KS-DFT over the whole range of Z_v . Actually, the two plots are almost indistinguishable in the graph. We note, however, that absolute difference in the kinetic energy at $Z_v = 2.2$ between the present work and the KS-DFT is evaluated as 0.006 a.u., and this is found to be about the half of the difference between them for the pseudo H atom at $Z_v = 0.8$.

In Fig. 5 the results for the pseudo Ne atom are plotted. The range of the energy variation is 1.5 times as large as that of the He atom. This is attributed to the fact that the

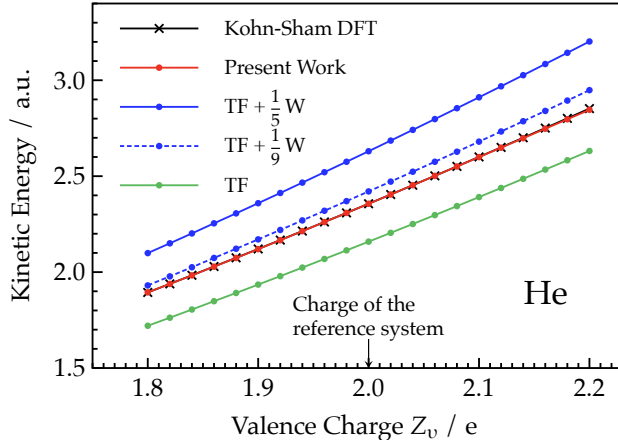


Figure 4: Plots of the kinetic energies computed by various kinetic functionals for the variation of the valence charge Z_v of the pseudo He atom. The atom with $Z_v = 2.0$ is taken as the reference system. The plots for ‘Kohn-Sham DFT’ and ‘Present Work’ are almost indiscernible in the figure. The other notations are the same as in Fig. 3.

number of the valence electrons for Ne is 4 times as many as that for He. Note, however, that the valence electrons in Ne reside outside the core region due to the repulsive potential $\Delta V_s(r)$ augmented in the local pseudopotential drawn in Fig. 1. Again, it is found that the coincidence between the present work and the KS-DFT is quite excellent. The maximum absolute deviation from the KS-DFT value is 0.006 a.u. that occurs at $Z_v = 7.8$. As a notable feature specific to the results for Ne, the Thomas-Fermi functional corrected with 1/9 Weizsäcker term shows good agreements with the KS-DFT in the range of $8.0 \leq Z_v \leq 8.2$.

Lastly, we provide the results for the pseudo Ar atom in Fig. 6. In the figure, it is shown that the range of the kinetic energy variation is reduced to about the half of the energy range for Ne. This can be attributed to the facts that the local pseudopotential of Ar (see Fig. 1) is much shallower than that of Ne, and the potential valley of Ar is located farther from the atomic core than that of Ne. It is worthy of noting that the present work shows the best agreements with the KS-DFT values in the application to Ar among the other atoms. Actually, the maximum deviation in the energy from the KS-DFT values is found to be only ~ 0.001 a.u. However, this is simply because the nonlocal energy gives the minor contribution to the kinetic energy in the Ar system. Explicitly, the nonlocal energy in the functional E_{kin}^e

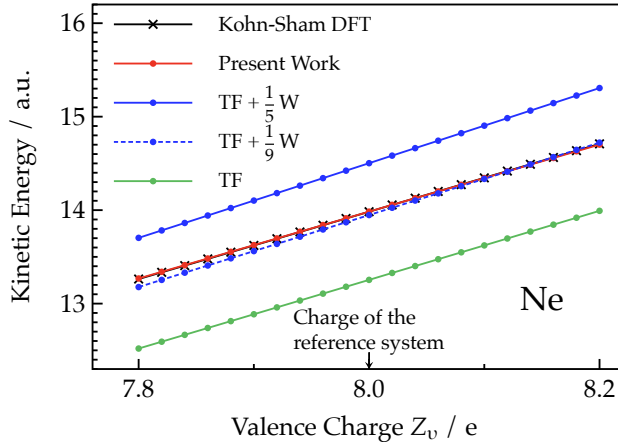


Figure 5: Plots of the kinetic energies computed by various kinetic functionals for the variation of the valence charge Z_v of the pseudo Ne atom. The atom with $Z_v = 8.0$ is taken as the reference system. The plots for ‘Kohn-Sham DFT’ and ‘Present Work’ are almost indiscernible in the figure. The other notations are the same as in Fig. 3.

of Eq. (20) is evaluated to be 0.007 a.u. at $Z_v = 8.2$.

We close this subsection by making a brief remark on the kinetic energy functional E_{kin}^e using a non self-consistent density. First, it was demonstrated that the functional is able to compute the kinetic energies with reasonable accuracies as compared with those obtained by the Kohn-Sham DFT. Second, it was found that the nonlocal term, represented with a functional of the energy electron density $n^e(\epsilon)$, certainly improves the description of the kinetic energy although the contribution to E_{kin}^e is proportional to the second order with respect to δn^e . In the next subsection, we provide the self-consistent densities obtained through the present OF-DFT approach.

4.2 Self-consistent Field Calculations with the OF-DFT Method

In this subsection, the radial distribution functions (RDFs) for electrons in the pseudo Ne and Ar atoms with $Z_v = 8.2$ are presented, where the corresponding electron densities are optimized through the self-consistent field (SCF) calculations utilizing Eqs. (31) and (32). The parameter η in Eq. (31) is set at 0.05. The convergence thresholds are 5.0×10^{-7} a.u. for the total energy, and 5.0×10^{-9} a.u.⁻³ for the density. The initial guess for the density for

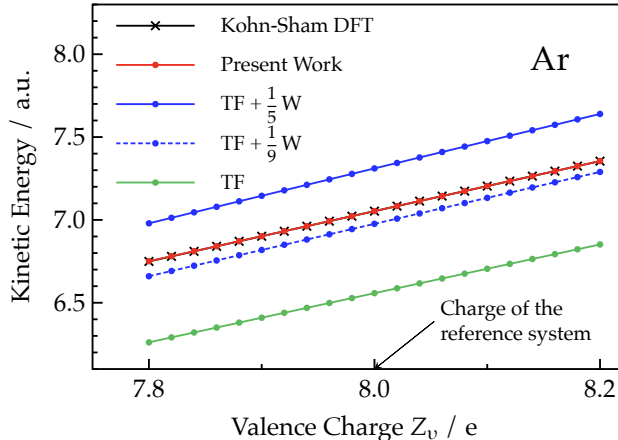


Figure 6: Plots of the kinetic energies computed by various kinetic functionals for the variation of the valence charge Z_v of the pseudo Ar atom. The atom with $Z_v = 8.0$ is taken as the reference system. The plots for ‘Kohn-Sham DFT’ and ‘Present Work’ are almost indiscernible in the figure. The other notations are the same as in Fig. 3.

each system is the electron density n_0 of the system with $Z_v = 8.0$. The 4-points polynomial interpolation method is utilized to increase the sampling points for the construction of the smooth RDFs. Explicitly, (100, 200, 400) grid points are yielded for the spherical coordinates (r, θ, ϕ) and the density on each grid is evaluated by the polynomial interpolation of the rectangular grids, where the range of the radial distance r is $0 \leq r \leq 8.604$ a.u. The results are plotted in Fig. 7. We found in the both plots that the RDFs optimized by the OF-DFT reasonably agree with those given by KS-DFT. We note, however, that the kinetic energies E_{kin} by the OF-DFT are somewhat different from those by KS-DFT calculations. Explicitly, E_{kin} for the Ne atom is evaluated as 14.685 a.u. by the OF-DFT, while the KS-DFT gives $E_{\text{kin}} = 14.709$ a.u. For the Ar atom, E_{kin} are computed as 7.344 and 7.355 a.u., by the OF-DFT and KS-DFT methods, respectively. Thus, it was found the kinetic energy as well as the density are degraded through the SCF procedure in the OF-DFT calculation. We note that the extreme agreements between the present works and the KS-DFT calculations in Figs. 5 and 6 can be attributed to the fact that the densities used for these calculations are obtained by the corresponding KS-DFT calculations.

We should make additional remarks on the construction of the RDF for the Ne atom.

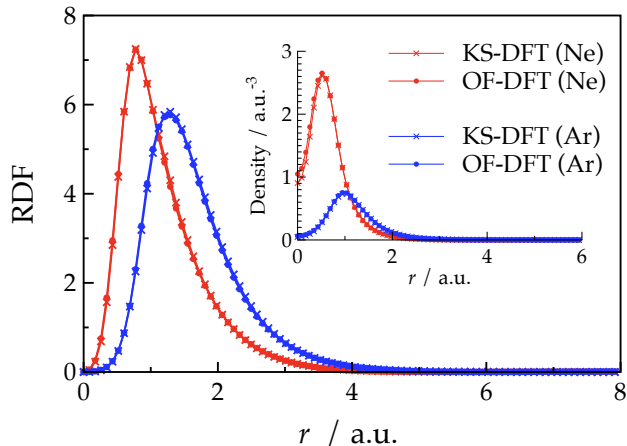


Figure 7: Plots of the radial distribution functions (RDFs) for the electrons in the pseudo Ne and Ar atoms. Superposed in the figure is the corresponding density profiles along the radial distance r . The electron densities are obtained through the SCF calculations. The valence charges Z_v of these systems are set at $Z_v = 8.2$ in the unit of the elementary charge.

Specifically in the SCF calculation for the Ne atom, we actually adopt the BHS local potential $V_{\text{loc}}^{\text{BHS}}(r)$ of the Ar atom[37] as the potential $v_{\text{def}}(\mathbf{r})$ to create the energy coordinate ϵ . The use of $V_{\text{loc}}^{\text{BHS}}(r)$ for Ne as $v_{\text{def}}(\mathbf{r})$ necessitates the wide energy range for the energy coordinate because the Ne potential is very steep around the atomic core. Therefore, in the construction of the response function using such a defining potential, a lot of bins become null in the region with large energy coordinate due to the low resolution of the real-space grids around the core. This might give rise to a numerical instability in the SCF calculation. In principle, the potential of any atomic core can be indeed used as a defining potential for another atom within the framework of the DFT based on the energy electron density[21] since the potential due to the nucleus is always spherically symmetric. Actually, the use of the Ar potential rather than the Ne potential in computing the plot in Fig. 5 makes a difference of only ~ 0.5 kcal/mol ($\sim 8 \times 10^{-4}$ a.u.) in the kinetic energy at $Z_v = 8.2$.

We also note an unfavorable phenomenon found in the SCF calculation for the Ne atom. That is, the electron population on the atomic core increases gradually through the SCF iterations, which seriously affects the density convergence. This suggests that the nonlocal term in the kinetic potential does not work appropriately on the atomic core region since only

the nonlocal potential is dependent on the electron density as seen in Eq. (18). The drawback might be attributed to the poor resolution of the grids around the core. The problem also emerges when $V_{\text{loc}}^{\text{BHS}}(r)$ for Ne is used as $v_{\text{def}}(\mathbf{r})$ because it also makes no contribution to increase the resolution around the core. Here, we apply an ad hoc approach to compensate for the error. Explicitly, we mix the kinetic potential with the Thomas-Fermi (TF) potential only on the core region using a Gaussian weight function $F(r)$. The explicit form of the kinetic potential \bar{v}_{kin}^e with the patch on the core is given by

$$\begin{aligned} \bar{v}_{\text{kin}}^e [n](\mathbf{r}) = & v_{\text{kin}} [n_0](\mathbf{r}) + F(r)v_{\text{kin}}^{\text{TF}} [n](\mathbf{r}) \\ & + (1 - F(r))v_{\text{kin}}^{\text{nlloc}} [n^e](\epsilon) \end{aligned} \quad (50)$$

where the potential $v_{\text{kin}}^{\text{nlloc}}$ is the second term of the right hand side of Eq. (18) and the weight function $F(r)$ is defined as

$$F(r) = \exp(-\zeta r^2) \quad (\zeta > 0) \quad (51)$$

In Eq. (50), the potential $v_{\text{kin}}^{\text{TF}} [n](\mathbf{r})$ is expressed in terms of the TF potential, thus,

$$v_{\text{kin}}^{\text{TF}} [n](\mathbf{r}) = \left. \frac{\delta v_{\text{TF}} [n](\mathbf{r})}{\delta n(\mathbf{r})} \right|_{n_0} (n(\mathbf{r}) - n_0(\mathbf{r})) \quad (52)$$

where the potential v_{TF} is given by the functional derivative of Eq. (1), that is, $\delta E_{\text{TF}} [n] / \delta n(\mathbf{r})$. Notice that the potential $v_{\text{kin}}^{\text{TF}} [n](\mathbf{r})$ is designed so that it becomes zero when the density $n(\mathbf{r})$ coincides with $n_0(\mathbf{r})$. The parameter ζ in Eq. (51) specifies the width of the Gaussian and it is set at $\zeta = 5.0 \text{ a.u.}^{-2}$ in the present calculation. With this choice of ζ , the weight $F(r)$ is reduced to less than 0.2 within the distance $r = 2h$ for the grid width of $h = 0.2868 \text{ a.u.}$ Thus, the potential $v_{\text{kin}}^{\text{TF}}$ in Eq. (50) applies only to the limited region around the core. It was demonstrated that the treatment improves the SCF convergence in the electron density. It was also found in the calculation of $Z_v = 8.2$ that the contribution of the TF energy to the kinetic energy amounts to 5.2 kcal/mol after the SCF convergence.

4.3 Covalent Bond in Hydrogen Molecule

As mentioned in subsection 3.5, the present method is also applied to the description of the covalent bond in a hydrogen molecule as a pilot test. The potential energy curve of the

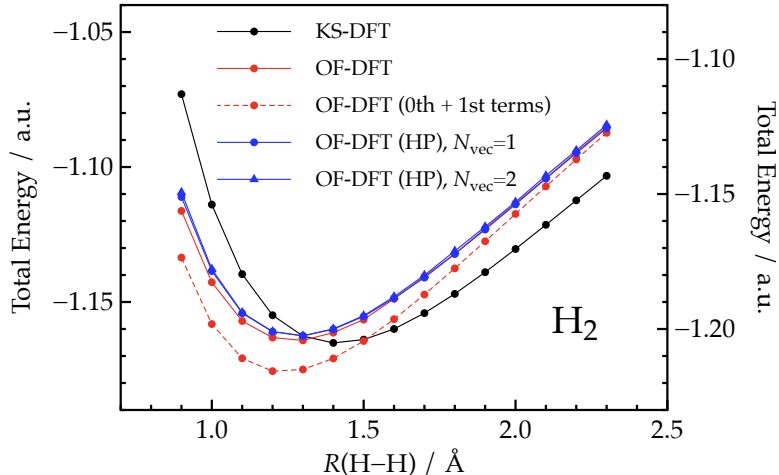


Figure 8: Plots of the potential energies of H_2 molecule computed by the present OF-DFT approach in comparisons with the one obtained by Kohn-Sham DFT with the BLYP functional. The notation ‘HP’ indicates that the component linear-response functions in Eq. (43) are each provided for the electron bound to harmonic potential, of which details are presented in subsection 3.5. The notation ‘ N_{vec} ’ indicates the number of eigenvectors included in the expansion of Eq. (41). The red broken line shows the potential energy curve obtained by Eq. (20) where the nonlocal term is excluded. The right axis is for the values of OF-DFT and shifted so that the bottoms of the curves almost match that of KS-DFT.

molecule around its equilibrium interatomic distance is provided in Fig. 8. The figure shows that the present OF-DFT calculation is able to describe the covalent bond of H_2 molecule although the equilibrium bond distance is shorter than that given by KS-DFT by 0.1 a.u. and the potential is deepened by ~ 0.035 a.u. The contribution of the nonlocal term in Eq. (20) to the potential energy is shown as the difference between the curves for ‘OF-DFT’ and ‘OF-DFT(0th + 1st terms)’ in the figure. The contribution gradually decreases as the interatomic distance R becomes larger as expected. It is also worthy of note in the figure that the use of the LRFs for the harmonic potential instead of the original electron-nuclear potential causes only a minor effect on the production of the curve. Since the LRF for the harmonic potential is built from the analytical functions as mentioned in subsection 3.5, the grid error due to the lack of the samplings does not exist at least. By taking advantage of this, we carry out the calculation including the eigenvector with the secondary largest

eigenvalue besides the largest one. However, it is found in the figure that the incorporation hardly affects the potential energy.

The remaining of this subsection is devoted to the discussion on the validity of the projection of the LRF onto the energy coordinate. As was demonstrated in Ref. [13], the formation of the shell structures in atomic densities was first realized in OF-DFT by the introduction of the nonlocal term to the kinetic energy functional besides the local and semi-local terms. Actually, the semi-local term (gradient or the second derivative) tends to reduce the density undulation since its operation relieves the distortion energy associated with the curvatures in the density. Thus, it seems that the nonlocal term is the critical component whereby the physically meaningful oscillations in the density can be reproduced.

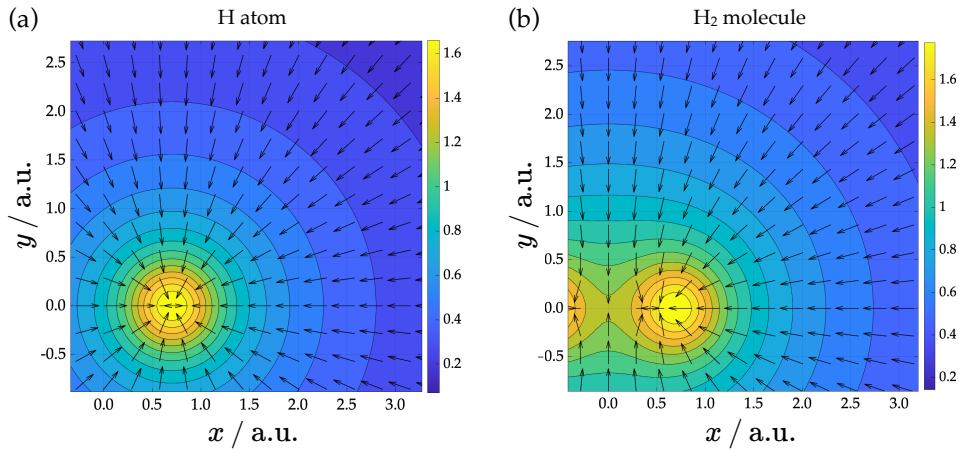


Figure 9: Superposition of the contour lines of the $v_{\text{def}}(\mathbf{r})$ and the vector field representation of the normalized gradient vectors $\nabla n(\mathbf{r})$ for (a) H atom, and (b) H₂ molecule. The contours are plotted for the values $\log(v_{\text{def}}(\mathbf{r})+1.0)$ with v_{def} evaluated by Eq. (33) and the normalized gradient vectors are provided on the real-space grids for the densities $n(\mathbf{r})$ optimized by Kohn-Sham DFT. The H atoms are placed at $x = -0.7$ and 0.7 a.u. on the x axis for the hydrogen molecule, while that is placed at $x = 0.7$ a.u. for the atomic system. The H atom is placed at $x = 0.7$ a.u. on the x axis for (a), while those are placed at $x = -0.7$ and 0.7 a.u. for (b).

The electron density oscillations, formed as a result of the equilibrium of the chemical potential of the electrons, will be induced along the direction parallel to the density gradient $\nabla n(\mathbf{r})$ of which absolute divided by $n(\mathbf{r})^{4/3}$ is often regarded as a measure of the electron density inhomogeneity. That is, the density wave emerges in the direction that causes the variation in the inhomogeneity of electrons. In the case of the atomic systems, where the density is spherically symmetric, the gradient vectors $n(\mathbf{r})^{4/3}$ are strictly parallel to the radial directions that are normal to the contour surface $\mathcal{R}_{\epsilon(\mathbf{r})}$ of the potential v_{def} . Therefore, the nonlocal operator can be represented on the radial coordinate r , or equivalently on the energy coordinate ϵ without loss of accuracy. To see this in more details, let us examine what happens when LRF $\chi_0(\mathbf{r}, \mathbf{r}')$ of Eq. (37) is reduced to $\chi_0(\epsilon, \epsilon')$ by means of Eq. (38). We consider the one-electron system, i.e. hydrogenic atom for the sake of simplicity. In the construction of $\chi_0(\mathbf{r}, \mathbf{r}')$ of H atom, p, d, f, \dots type orbitals besides the s orbital are to be included in the summation of the excited states in Eq. (37). However, the products $\varphi_i^*(\mathbf{r})\varphi_a(\mathbf{r})$ except for the terms due to $1s \rightarrow ns$ type transitions completely vanish when they are integrated over the contour surface $\mathcal{R}_{\epsilon(\mathbf{r})}$ due to the orthogonality of the spherical harmonic functions. The same is true for the products $\varphi_i^*(\mathbf{r}')\varphi_a(\mathbf{r}')$ on the region $\mathcal{R}_{\epsilon(\mathbf{r}')}$. It is thus revealed that only the $1s \rightarrow ns$ transitions contribute to the construction of $\chi_0(\epsilon, \epsilon')$. However, this does not mean that the LRF is degraded due to the projection because the polarization created by the transition e.g. from s to p orbital should be excluded in the formation of the spherically symmetric density. The polarizations due to $1s \rightarrow ns$ type transitions are thus suffice to describe the density oscillation in the atom.

The above discussion can be generalized to molecular systems. Figure 9(a) shows the contours of the potential $v_{\text{def}}(\mathbf{r})$ for an isolated hydrogen atom, on which the vector field for the gradient $\nabla n(\mathbf{r})$ of the atom is also superposed. Each gradient vector on a contour line is, of course, strictly normal to the line. Figure 9(b), on the other hand, shows its counterpart of the molecular system, i.e. hydrogen molecule with the interatomic distance $R = 1.4$ a.u. It is also seen in the figure that the gradient vectors on the contours are almost normal to the lines. This is indicative of the fact that the contours of the electron density of H_2 are almost parallel to those of the potential $v_{\text{def}}(\mathbf{r})$ as suggested by Parr and Berk[25]. As was mentioned for the atomic system the density oscillation is induced along the gradient

of the density, or equivalently along the direction normal to the contour surfaces of the potential $v_{\text{def}}(\mathbf{r})$. Then, it is quite reasonable to anticipate that the density oscillations in the molecular system also arises along the direction that corresponds to the variation in the energy coordinate. Therefore, the LRF $\chi_0(\mathbf{r}, \mathbf{r}')$ for the molecular system can be reasonably reduced to $\chi_0^e(\epsilon, \epsilon')$ through the projection onto the energy coordinate.

In closing this subsection we make a comment on the advantage of the LRF represented on the energy coordinate in comparison with that on the real space. First of all, the LRF $\chi_0(\mathbf{r}, \mathbf{r}')$ is the 6-dimensional matrix and may be handled numerically. Even when the LRF is given, the inversion of it is seemingly infeasible. A remedy to solve the problem is to introduce a certain basis set to represent the matrix although any proper choice of it is not known. We also note that the numerical cost scales as $O(N^2)$ with the number N included in the system. In contrast, the cost associated with the handling of $\chi_0^e(\epsilon, \epsilon')$ stays constant with respect to the system size as long as the energy range is not changed. Anyway, the computational cost as well as the accuracy of the molecular LRF are deeply dependent on the method to build it. The assessment of these issues will be carried out in the future works.

5 Conclusion and Perspective

In this article, we developed a kinetic energy functional $E_{\text{kin}}^e[n]$ within the framework of the density-functional theory based on the energy electron density $n^e(\epsilon)$ [21] for the purpose of realizing the orbital-free DFT(OF-DFT) calculations. The functional includes the nonlocal term described with a linear-response function(LRF) of a reference system as was introduced in the Wang-Teter functional[13]. As a notable feature, the LRF, which constitutes the integral kernel of the nonlocal term, is represented on the energy coordinate ϵ , thus, $\chi_0^e(\epsilon, \epsilon')$. In addition, an atomic system is taken as a reference system in contrast to the conventional approach that utilizes LRF of the homogeneous electron gas. The kinetic functional $E_{\text{kin}}^e[n]$ was formulated by means of the coupling-parameter integration scheme. The functional was applied to the calculation of the kinetic energies of the pseudo atoms which stem from H, He, Ne, and Ar atoms. Explicitly, the kinetic energy of each atom was computed with respect to the variation of the valence charge Z_v , where the atom with its original charge Z_v was adopted

as the reference system to construct $\chi_0^e(\epsilon, \epsilon')$. It was demonstrated that the functional $E_{\text{kin}}^e[n]$ is able to provide the kinetic energies in good agreements with those obtained by the Kohn-Sham DFT(KS-DFT) for the given non self-consistent electron densities n .

We also devised a scheme to perform the self-consistent field (SCF) calculation using $E_{\text{kin}}^e[n]$ although the sophistications to expedite the convergence were not made. The radial distribution functions (RDFs) of the electrons in the pseudo Ne and Ar with $Z_v = 8.2$ were obtained through the SCF calculations. The RDFs by the OF-DFT calculations showed reasonable agreements with those given by KS-DFT calculations. Thus, the reliability of the method was demonstrated.

The present method is also applied to the calculation of a covalent bond in H_2 molecule as a pilot system. To ensure that OF-DFT makes sense, it is essential to make the computational cost to increase linearly with the system size. Our strategy to solve the problem is to compute and store beforehand the LRFs of the constituent atoms. Then, we make the overlap of the component LRFs on the energy coordinate to construct the total LRF of the molecule. This is, of course, an instantaneous and straightforward approach to model the LRF of the molecular systems. The reference electron density n_0 will also be constructed from the overlap of the electron densities of the individual atoms. It was found that the potential energy curve of H_2 molecule is reasonably reproduced by such a crude model. The analyses of the property of the LRF or its improvements will be the subject of the forthcoming issues. We note that the construction of the molecular LRF on the energy coordinate is justified by the DFT based on the energy electron density[21]. Although the projection of the LRF onto the energy coordinate itself is time consuming, the computational cost is proportional to the system size.

Acknowledgments

The author is grateful to Prof. N. Matubayasi in Osaka university for the fruitful discussions on the pseudo inverse method utilized for the inversion of the linear-response matrix. This paper was supported by the Grant-in-Aid for Scientific Research on Innovative Areas (No. 23118701) from the Ministry of Education, Culture, Sports, Science, and Technology

(MEXT); the Grant-in-Aid for Challenging Exploratory Research (No. 25620004) from the Japan Society for the Promotion of Science (JSPS); and the Grant-in-Aid for Scientific Research(C) (No. 17K05138) from the Japan Society for the Promotion of Science (JSPS). This research also used computational resources of the HPCI system provided by Kyoto, Nagoya, and Osaka university through the HPCI System Research Project (Project IDs: hp170046, hp180030, hp180032, hp190011, and hp200016).

Appendix

A Linear-response Function

Here, we prove that the linear-response function (LRF) $\chi_0^e(\epsilon, \epsilon')$ in Eq. (19) defined on the energy coordinate is positive semi-definite. We start the discussion with the LRF $\chi_0(\mathbf{r}, \mathbf{r}')$ in Eq. (37) defined on the spatial coordinate. First, we provide the proof that $\chi_0(\mathbf{r}, \mathbf{r}')$ is positive semi-definite. To this end, we consider a quantity Q with respect to an arbitrary function $q(\mathbf{r})$,

$$Q = \int d\mathbf{r}d\mathbf{r}' q(\mathbf{r})\chi_0(\mathbf{r}, \mathbf{r}') q^*(\mathbf{r}') \quad (53)$$

For our purpose, it is sufficient to prove that the relation $Q \geq 0$ always holds. By substituting Eq. (37) into Eq. (53), one readily obtains,

$$\begin{aligned} Q &= \int d\mathbf{r}d\mathbf{r}' \sum_i^{\text{occ}} \sum_a^{\text{vir}} \frac{1}{\epsilon_a^0 - \epsilon_i^0} q(\mathbf{r})\varphi_i^{0*}(\mathbf{r})\varphi_a^0(\mathbf{r}) \times \varphi_a^{0*}(\mathbf{r}')\varphi_i^0(\mathbf{r}')q^*(\mathbf{r}') \\ &= \sum_i^{\text{occ}} \sum_a^{\text{vir}} \frac{1}{\epsilon_a^0 - \epsilon_i^0} \int d\mathbf{r}d\mathbf{r}' \Phi_{ia}(\mathbf{r})\Phi_{ia}^*(\mathbf{r}') \\ &= \sum_i^{\text{occ}} \sum_a^{\text{vir}} \frac{1}{\epsilon_a^0 - \epsilon_i^0} |S_{ia}|^2 \end{aligned} \quad (54)$$

where the function $\Phi_{ia}(\mathbf{r})$ in the right hand side of the second equality is defined as $\Phi_{ia}(\mathbf{r}) = q(\mathbf{r})\varphi_i^{0*}(\mathbf{r})\varphi_a^0(\mathbf{r})$ and S_{ia} in the last equality is given by $S_{ia} = \int d\mathbf{r}\Phi_{ia}(\mathbf{r})$. Note that the quantity Q becomes zero when the function $q(\mathbf{r})$ is constant. Thus, it is proved that $\chi_0(\mathbf{r}, \mathbf{r}')$ is positive semi-definite. Then, the it is rather straightforward to prove that $\chi_0^e(\epsilon, \epsilon')$ is also

positive semi-definite. For an arbitrary function $q^e(\epsilon)$, it reads,

$$\begin{aligned}
& \int d\epsilon d\epsilon' q^e(\epsilon) \chi_0^e(\epsilon, \epsilon') q^e(\epsilon') \\
&= \int d\epsilon d\epsilon' q^e(\epsilon) q^e(\epsilon') \\
&\quad \times \int d\mathbf{r} d\mathbf{r}' \chi_0(\mathbf{r}, \mathbf{r}') \delta(\epsilon - v(\mathbf{r})) \delta(\epsilon' - v(\mathbf{r}')) \\
&= \int d\mathbf{r} d\mathbf{r}' \chi_0(\mathbf{r}, \mathbf{r}') \int d\epsilon q^e(\epsilon) \delta(\epsilon - v(\mathbf{r})) \int d\epsilon' q^e(\epsilon') \delta(\epsilon' - v(\mathbf{r}')) \\
&= \int d\mathbf{r} d\mathbf{r}' \theta(\mathbf{r}) \chi_0(\mathbf{r}, \mathbf{r}') \theta(\mathbf{r}') \geq 0
\end{aligned} \tag{55}$$

where $\theta(\mathbf{r})$ is defined as $\int d\epsilon q^e(\epsilon) \delta(\epsilon - v(\mathbf{r}))$. Thus, $\chi_0^e(\epsilon, \epsilon')$ is also positive semi-definite. Hence, $\chi_0^e(\epsilon, \epsilon')$ can be inverted through a manipulation such as a pseudo inverse method.

B Grid Error in Response Function

Since we utilize the real-space grid (RSG) approach in representing the response function $\chi_0(\mathbf{r}, \mathbf{r}')$, its projection $\chi_0^e(\epsilon, \epsilon')$ onto the energy coordinate ϵ (Eq. (19)) is affected by the grid error inherent in $\chi_0(\mathbf{r}, \mathbf{r}')$. In this Appendix, we demonstrate that the terms with small eigenvalues in the spectral decomposition in Eq. (40) are comparable in magnitude to the grid error in $\chi_0^e(\epsilon, \epsilon')$. To this end, we employ the double-grid technique. Explicitly, the values $\chi_0(\mathbf{r}, \mathbf{r}')$ at the double grids (DGs) are evaluated through numerical interpolations of the original coarse grids (CGs) to save the computer resources. In the next paragraph, a concise explanation is provided for the DG method applied to the response function of the Ar atom.

Hereafter, it is assumed that the origin of the position vectors is set at the atomic center. Since $\chi_0(\mathbf{r}, \mathbf{r}')$ as a function of \mathbf{r} has a cylindrical symmetry around the axis Z being oriented to the vector \mathbf{r}' , the original data $\chi_0(\mathbf{r}, \mathbf{r}')$ at CGs, which serve to evaluate the response function at DGs, can be reduced to three-dimensional data $\tilde{\chi}_0$ without losing the information contents. Explicitly, the reference response function $\tilde{\chi}_0$ has the three arguments, thus $\tilde{\chi}_0(d; Y, Z)$, where d represents the length of the vector \mathbf{r}' , and the coordinates (Y, Z) specify the position \mathbf{r} on the plane which includes \mathbf{r} and the axis Z . We, thus evaluate $\tilde{\chi}_0(d; Y, Z)$ beforehand at CGs with the grid width h given in subsection 3.1. The DGs are then placed

within each CG at the interval of h/N_{DG} along each axis ($1 \leq N_{\text{DG}} \leq 4$, $N_{\text{DG}} \in \mathbb{Z}$). Let \mathbf{r}_i and \mathbf{r}_j be the position vectors of the DGs with indices i and j , respectively, the corresponding response function $\chi_0(\mathbf{r}_i, \mathbf{r}_j)$ is to be obtained through the following procedure. Based on the above discussion, the six-dimensional coordinate $(\mathbf{r}_i, \mathbf{r}_j)$ can be readily cast into the reduced variables $(d; Y, Z)$, thus

$$\begin{cases} d = |\mathbf{r}_j| \\ Y = |\mathbf{r}_i| \sin \theta \\ Z = |\mathbf{r}_i| \cos \theta \end{cases} \quad (56)$$

where θ represents the angle between the vectors \mathbf{r}_i and \mathbf{r}_j , and defined by $\cos \theta = \frac{\mathbf{r}_i \cdot \mathbf{r}_j}{|\mathbf{r}_i| |\mathbf{r}_j|}$. We note that the indices i and j in Eq. (56) are interchangeable because of the symmetry of the function $\chi_0(\mathbf{r}_i, \mathbf{r}_j)$. In this work, the response function $\chi_0(\mathbf{r}_i, \mathbf{r}_j)$ between the coordinates \mathbf{r}_i and \mathbf{r}_j at the DGs is evaluated through the 4th-order polynomial interpolation of the function $\tilde{\chi}_0(d; Y, Z)$ defined at CGs. The DGs are placed within the CGs of which distances from the atomic core are less than 5.0 a.u. The numerical detail of the interpolation is presented in Ref. [28].

In Fig. 10 the diagonal elements of the response functions $\chi_0^e(\epsilon, \epsilon')$ as functions of the index for the discrete energy coordinate ϵ are presented for the various N_{DG} . It is seen in the figure that all the graphs are characterized by two distinct peaks although they differ slightly each other due to the difference in the width of the DG. It is also recognized that the graphs reasonably converge as the grid interval decreases, which shows that the calculation with $N_{\text{DG}} = 4$ offers the smallest grid error among the plots as expected. We subtract the result for $N_{\text{DG}} = 4$ from that for other N_{DG} to estimate the effect of the grid width on the response function. Since the result for $N_{\text{DG}} = 1$ is equivalent in principle to the calculation done in the main text, the graph ' $N_{\text{DG}}(1) - N_{\text{DG}}(4)$ ' approximately exhibits the grid error in representing $\chi_0^e(\epsilon, \epsilon')$ in the present work. The three horizontal broken lines in the figure approximately show maximum values of the plots shown in Figs. 2(b), (c), and (d). It is observed that the grid error is comparable or even larger in magnitude than the response functions with g_2 and g_3 . Therefore, the high-frequency modes γ_i in the response function are seriously contaminated by artifacts due to the grid errors. These contributions should be excluded from the summation of Eq. (41) because the contamination is erroneously

amplified by the multiplication of g_i^{-1} . Seemingly, it is quite difficult to extract the grid errors from the eigenvectors. One might consider that the DG method will alleviate the problem. We found, however, that the introduction of the DGs destroys unfortunately the crucial condition that $\chi_0^e(\epsilon, \epsilon')$ is positive semi definite. This problem could be attributed to the error in the polynomial interpolation utilized in the DG method.

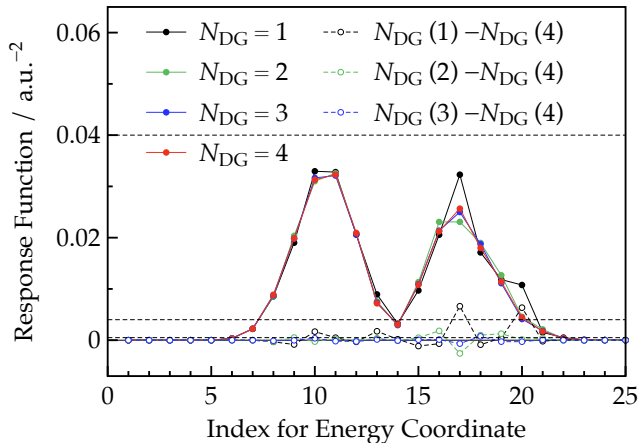


Figure 10: The diagonal elements of the linear-response function $\chi_0^e(\epsilon, \epsilon')$ for the pseudo Ar atom as functions of the grid index for the energy coordinate ϵ . The real lines are the plots for the calculations with N_{DG} . The plots with the broken lines are the results for $N_{\text{DG}} = 1, 2$, and 3 subtracted by that for $N_{\text{DG}} = 4$. The three horizontal broken lines represent the values, 0.04 , 0.004 , and 0.0005 , which are approximately the maximum values of the component response functions $g_i \gamma_i(\epsilon) \gamma_i(\epsilon')$ with the eigenvalues g_1 , g_2 , and g_3 shown in Figs. 2(b), (c), and (d), respectively.

Although the truncation in the expansion of Eq. (40) within a few terms would not seriously affect the accuracy of the kinetic energy, it is desirable to make some devices in the future work to alleviate the problem. First, some approximate method should be developed to estimate the error in the response function in terms of the grid size in the real-space cell, which will offer a method of rational truncations. Second, a new numerical device for the DG approach should be made to maintain the positive semi definiteness in the construction of the matrix $\chi_0^e(\epsilon, \epsilon')$. These subjects will be addressed in the forthcoming issues.

References

1. R. G. Parr and W. Yang, *Density-functional theory of atoms and molecules* (Oxford university press, New York, 1989).
2. R. M. Martin, *Electronic Structure, Basic Theory and Practical Methods* (Cambridge University Press, Cambridge, 2004).
3. E. Engel and R. M. Dreizler, *Theoretical and Mathematical Physics, Density Functional Theory* (Springer, Heidelberg, 2011).
4. M. Levy, Proc. Natl. Acad. Sci, USA **76**, 6062 (1979).
5. W. Kohn and L. J. Sham, Phys. Rev. **140**, A1133 (1965).
6. T. A. Wesolowski and Y. A. Wang, eds., *Recent Progress in Orbital Free Density Functional Theory (Recent Advances in Computational Chemistry)* (World Scientific, Singapore, 2013).
7. L. H. Thomas, Proc. Camb. Phil. Soc. **23**, 541 (1927).
8. E. Fermi, Z. Phys. **48**, 73 (1928).
9. C. F. von Weizsacker, Z. Phys. **96**, 431 (1935).
10. Y. A. Wang and E. A. Carter, *Chapter 5 in Theoretical Methods in Condensed Phase Chemistry (Progress in Theoretical Chemistry and Physics)*, vol. 5 (Kluwer, Dordrecht, 2000).
11. K. Yonei and Y. Tomishima, J. Phys. Soc. Jpn. **20**, 1051 (1965).
12. E. Chacón, J. E. Alvarellos, and P. Tarazona, Phys. Rev. B **32**, 7868 (1985).
13. L.-W. Wang and M. P. Teter, Phys. Rev. B **45**, 13196 (1992).
14. Y. A. Wang, N. Govind, and E. A. Carter, Phys. Rev. B **58**, 13465 (1998).
15. Y. A. Wang, N. Govind, and E. A. Carter, Phys. Rev. B **60**, 350 (1999).

16. C. Huang and E. A. Carter, *Phys. Rev. B* **81**, 1 (2010).
17. W. Mi, A. Genova, and M. Pavanello, *J. Chem. Phys.* **148** (2018).
18. W. Mi and M. Pavanello, *Phys. Rev. B* **100**, 1 (2019).
19. L. A. Constantin, E. Fabiano, and F. Della Sala, *Phys. Rev. B* **97**, 1 (2018).
20. W. C. Witt, B. G. Del Rio, J. M. Dieterich, and E. A. Carter, *J. Mater. Res.* **33**, 777 (2018).
21. H. Takahashi, *J. Phys. B: At. Mol. Opt. Phys.* **51**, 055102(11pp) (2018).
22. P. Hohenberg and W. Kohn, *Phys. Rev.* **136**, B864 (1964).
23. H. Takahashi, *J. Phys. B: At. Mol. Opt. Phys.* **53**, 245101(9pp) (2020).
24. J. Lindhard, *Kgl. Danske Videnskab. Selskab Mat.-fys. Medd.* **28** (1954).
25. R. G. Parr and A. Berk, in *Chemical Applications of Atomic and Molecular Electrostatic Potentials*, edited by P. Politzer and D. G. Truhlar (Plenum Press, 1981), pp. 51–62.
26. N. Matubayasi and M. Nakahara, *J. Chem. Phys.* **119**, 9686 (2003).
27. H. Takahashi, T. Hori, T. Wakabayashi, and T. Nitta, *Chem. Lett.* **3**, 222 (2000).
28. H. Takahashi, T. Hori, T. Wakabayashi, and T. Nitta, *J. Phys. Chem. A* **105**, 4351 (2001).
29. H. Takahashi, T. Hori, H. Hashimoto, and T. Nitta, *J. Comp. Chem.* **22**, 1252 (2001).
30. H. Takahashi, N. Matubayasi, M. Nakahara, and T. Nitta, *J. Chem. Phys.* **121**, 3989 (2004).
31. H. Takahashi, D. Suzuoka, S. Sakuraba, and A. Morita, *J. Phys. Chem. B* **123**, 7081 (2019).
32. H. Takahashi, S. Sakuraba, and A. Morita, *Journal of Chemical Information and Modeling* **60**, 1376 (2020).

33. J. R. Chelikowsky, N. Troullier, K. Wu, and Y. Saad, Phys. Rev. B **50**, 11355 (1994).
34. J. R. Chelikowsky, N. Troullier, and Y. Saad, Phys. Rev. Lett. **72**, 1240 (1994).
35. A. D. Becke, Phys. Rev. A **38**, 3098 (1988).
36. C. Lee, W. Yang, and R. G. Parr, Phys. Rev. B **37**, 785 (1988).
37. G. B. Bachelet, D. R. Hamann, and M. Schluter, Phys. Rev. B **26**, 4199 (1982).
38. T. Ono and K. Hirose, Phys. Rev. Lett. **82**, 5016 (1999).
39. T. A. Wesolowski, S. Shedge, and X. Zhou, Chem. Rev. **115**, 5891 (2015).
40. T. A. Wesolowski, H. Chermette, and J. Weber, J. Chem. Phys. **105**, 9182 (1996).
41. T. A. Wesolowski, J. Chem. Phys. **106**, 8516 (1997).
42. P. De Silva and T. A. Wesolowski, J. Chem. Phys. **137** (2012).
43. L. Kleinman and D. M. Bylander, Phys. Rev. Lett. **48**, 1425 (1982).
44. A. Szabo and N. S. Ostlund, *Modern Quantum Chemistry* (Macmillan, New York, 1982).
45. S. G. Nilsson and I. Ragnarsson, *Shapes and Shells in Nuclear Structure* (Cambridge University Press, 1995).
46. A. J. Thakkar, Phys. Rev. A **46**, 6920 (1992).